TIME-FREQUENCY ANALYSIS OF EEG

TIME-FREQUENCY ANALYSIS OF ELECTROENCEPHALOGRAPHIC ACTIVITY IN THE ENTORHINAL CORTEX AND HIPPOCAMPUS

By

YAN XU
B.Sc. (Zhejiang University)
M.Sc. (Queen's University)

A Thesis
Submitted to the School of Graduate Studies
in Partial Fulfilment of the Requirements
for the Degree
Master of Engineering

McMaster University

MASTER OF ENGINEERING (1997) MCMASTER UNIVERSITY
(Electrical and Computer Engineering) Hamilton, Ontario

TITLE: **Time-Frequency Analysis of Electroencephalographic Activity in the Entorhinal Cortex and Hippocampus**

AUTHOR: Yan Xu
B.Sc. (Zhejiang University)
M.Sc. (Queen's University)

SUPERVISOR: Dr. Simon Haykin

NUMBER OF PAGES: xii, 56

Abstract

Oscillatory states in the Electroencephalogram (EEG) reflect the rhythmic synchronous activation in large networks of neurons. Time-frequency methods quantify the spectral content of the EEG as a function of time. As such, they are well suited as tools for the study of spontaneous and induced changes in oscillatory states. We have used time-frequency techniques to analyze the flow of activity patterns between two strongly connected brain structures: the entorhinal cortex and the hippocampus, which are believed to be involved in information storage.

EEG was recorded simultaneously from the entorhinal cortex and the hippocampus of behaving rats. During the recording, low-intensity trains of electrical pulses at frequencies between 1 and 40 Hz were applied to the olfactory (piriform) cortex. The piriform cortex projects to the entorhinal cortex, which then passes the signal on to the hippocampus. Several time-frequency methods, including the short-time Fourier transform (STFT), Wigner-Ville distribution (WVD) and multiple window (MW) time-frequency analysis (TFA), were used to analyse EEG signals. To monitor the signal transmission between the entorhinal cortex and hippocampus, the time-frequency coherence functions were used. The analysed results showed that stimulation-related power in both sites peaked near 15 Hz, but the coherence between the EEG signals recorded from these two sites increased monotonically with stimulation frequency.

Among the time-frequency methods used, the STFT provided time-frequency distributions not only without cross-terms which were present in the WVD, but also with higher resolutions in both time and frequency than the MW-TFA. The STFT seems to be the most suitable time-frequency method to study the stimulation-induced signals presented in this thesis. The MW-TFA, which gives low bias and low variance estimations of the time-frequency distribution when only *one realization* of data is given, is suitable for stochastic and nonstationary signals such as spontaneous EEG. We also compared the performance of the MW-TFA using two different window functions: Slepian sequences and Hermite functions. By carefully matching the two window functions, we found no noticeable difference in time-frequency plane between them .

Acknowledgements

I would like to sincerely thank Dr. Simon Haykin for supervising this Thesis and my other research efforts. I am grateful to Dr. Ronald J. Racine, co-supervisor of my research activities, for his guidance and inspiration.

I take this opportunity to thank Dr. C. Andrew Chapman for his help in data collection and thoughtful discussions on the experimental results.

Finally, I extend my gratitude to my husband, Jun, for his full support and encouragement.

Contents

List of Figures

Glossary

Neurobiology Terms

Dentate gyrus: A major component of the hippocampus that receives extensive cortical input via the entorhinal cortex.

Electroencephalogram: A recording of the electrical activity of brain through surface or implanted electrodes.

Entorhinal cortex: A cortical region surrounding the hippocampus which receives processed cortical information and sends it on to the hippocampus (dentate gyrus).

Hippocampus: A brain structure receives processed information from several different sensory systems.

Neuron: A cell in the nervous system that is organized to generate and transmit electrochemical signals.

Olfactory bulb: The brain structure that receives input from olfactory receptors.

Piriform cortex: The area of the brain that receives input from the olfactory bulb; this area is also referred to as olfactory cortex.

Stimulus binding: The linking of individual neuronal representations of different, local features of external stimuli by a common oscillatory pattern of discharge.

Synapse: The connection between neurons, via which an electrochemical signal is transmitted.

Abbreviations

EEG: electroencephalogram

ED: exponential distribution

MW: multiple window

MWM: multiple window method

RID: reduced interference distribution

STFT: short-time Fourier transform

TFA: time-frequency analysis

WT: wavelet transform

WVD: Wigner-Ville distribution

Chapter 1

Introduction

One of the great challenges in neurobiology is the understanding of how sensory information is represented by spatiotemporal patterns of neuronal activity and how these representations are transmitted from one brain region to another during their further elaboration and processing (Hebb, 1949). The measurement of electrical brain activity, and its correlates with behavior, can provide us with useful clues about these processes. Unfortunately, current technology does not allow us to record the individual activities of more than about 50 neurons at a time (and very few laboratories around the world are able to record from more than three or four). With such small numbers of cells sampled, there is little that we can say about the nature of the networks of millions of cells that mediate cognitive functions.

The alternative to multiunit recording is the use of large electrodes to record the summed electrical activity of very large numbers of neurons (the EEG) (Berger, 1929). While the spatial resolution of the EEG is poor, the temporal resolution is quite good and can provide us with some insights into the activity of large networks of neurons. Spontaneously occurring EEG can be used to monitor the activity of neuronal networks during naturally occurring behaviors (Knott et al., 1842; Scheuler et al., 1990), and changes in EEG activity following the presentation of experimentally controlled stimuli can offer further insights into the processes of perception, learning, and memory (Ehlers et al., 1987). Such stimuli could range from relatively normal sensory (e.g., auditory or visual) signals to the application of electrical stimulation directly to brain sites through implanted electrodes. Both spontaneous and evoked EEG activity can be oscillatory in nature, and EEG recordings are used extensively to monitor neuronal activation patterns, and the flow of neuronal signals between brain sites.

EEG time series usually contain multiple frequency components, which vary spontaneously and in response to experimental manipulations. Further, these data sets can be quite large, especially when multiple brain sites are sampled in studies of the relationships between EEG activity in connected regions of the brain. This necessitates the need for effective techniques for the analysis of these large data sets. In this thesis, we explore the application of time-frequency analysis (TFA) techniques to the description of the genesis and propagation of oscillatory EEG activity in brain sites believed to be involved in information storage. We have used these techniques to monitor the responsiveness of particular brain sites to rhythmic stimulation. We have also used coherence analysis to measure the transmission of induced signals between brain sites.

This thesis is organized as follows: Chapter 2 gives a biological background of EEG signals and the brain sites where EEG is measured. Chapter 3 explains briefly experimental set-up procedures and data collecting methods. Chapter 4 introduces conventional time-frequency analysis methods, describes the application of TFA to experimental data, and reports major experimental results. Chapter 5 is devoted to multiple window (MW) time-frequency analysis (TFA). The application of MW-TFA to experimental data and a comparison of MW-TFA using two sets of window functions are given in this chapter. The final conclusions are covered in Chapter 6.

Chapter 2

EEG Signals

2.1 Introduction

EEG signals result from the combined electrical activity of very large numbers of neurons. Synaptic communication between neurons results in the activation of the post-synaptic cell by the flow of small current across the dendritic membrane of the post-synaptic cell. The membrane currents give rise to potential differences which are generally referred to as field potentials. The neuronal elements in the brain are embedded within the conductive extracellular medium. Therefore, the volume conducted field potentials can be recorded from the scalp in human objects, or from electrodes implanted into specific brain regions in experimental animals. If the activated membrane regions across neurons are spatially diffuse, the spatial averaging of the many membrane currents in the extracellular space reduces the amplitude of the EEG. However, when many cells of the same type are activated simultaneously via synapses in the same local region, the resulting field potentials can add up spatially and result in relatively large amplitude EEG signals.

EEG signals provide an effective method for monitoring the dynamics of spontaneous or stimulus driven neuronal activity with extreme temporal resolution. EEG-based measures can reflect both the temporal nature of neuronal activity within one site, and the relationships between neuronal activity in sites linked by multiple synapses. Although the EEG signal can be recorded with arbitrary temporal resolution, it has poor spatial resolution. The populations of cells which contribute to the recorded EEG and their distance from the recording electrode are not always well understood.

2.2 Temporal Processing of EEG Signals

Oscillatory states are the most striking feature of EEG activity because they reflect not only the synchronization of massive numbers of neurons, but also a temporally-ordered rhythmicity of activation (Lopes da Silva, 1991). Rhythmic synchronization can result either from intrinsic oscillatory properties of individual neurons or from synaptic interactions in networks of neurons and the action of neuromodulatory systems (Lopes da Silva, 1991; Steriade et al., 1990). Oscillatory states in EEG activity fall into distinct categories that are discriminable by the amplitude and frequency ranges of the oscillation, the brain sites in which they may be observed, and the underlying neural mechanisms which serve to generate the oscillations. In scalp recorded normal human EEG, there are distinct oscillatory rhythms distinguishable by frequency and are commonly referred to as delta (0.5–4 Hz), theta (4–8 Hz), alpha (8–13 Hz) and beta (13–30 Hz) (Dutertre, 1974; Michel et al., 1992). Analogous rhythms are also observed in experimental animals at slightly different frequencies which depend on the species and preparation (Bland, 1986; Hogan and Fitzpatrick, 1988).

Because oscillatory states in the EEG reflect ordered temporal patterns of synchronous neural activity within and between brain areas, a common notion is that different oscillatory states may be indicative of distinct information processing states in which the oscillatory patterns play an active role. This agrees with current theoretical notions which emphasize the role of both spatial and temporal aspects of processing in neuronal computation (Hebb, 1949; Lopes da Silva, 1991; Singer, 1993). These notions hold that the rhythmic synchronization during oscillatory states can serve to enhance perception, learning, and the transmission of neuronal signals between different regions of the brain.

2.3 Oscillatory Patterns in the Hippocampus and Olfactory System EEG

In this thesis, we studied the transmission of neuronal signals from the entorhinal cortex to the hippocampus. The hippocampus is a brain structure involved in spatial memory and the integration of sensory information. The entorhinal cortex and the hippocampus are strongly connected. Much of the information the hippocampus receives from cortical areas, including the olfactory (piriform) cortex, is funnelled through the entorhinal cortex (Witter et al., 1889) (Fig. 2.1). There are all types of sensory information communicating between the entorhinal cortex and the hippocampus and different information may have different representations. We have chosen to monitor the transmission of olfactory inputs from the piriform cortex to these two structures. The piriform cortex input to the entorhinal cortex is not only one of its largest inputs, but also it carries putatively unimodal sensory (olfactory) information (Lopes da Silva et al., 1990). This allows a less ambiguous interpretation of the types of sensory information that could be involved in the signal transmission.

The hippocampus and olfactory system display a variety of oscillatory rhythms related to signal transmission between brain regions. The most prominent rhythm in

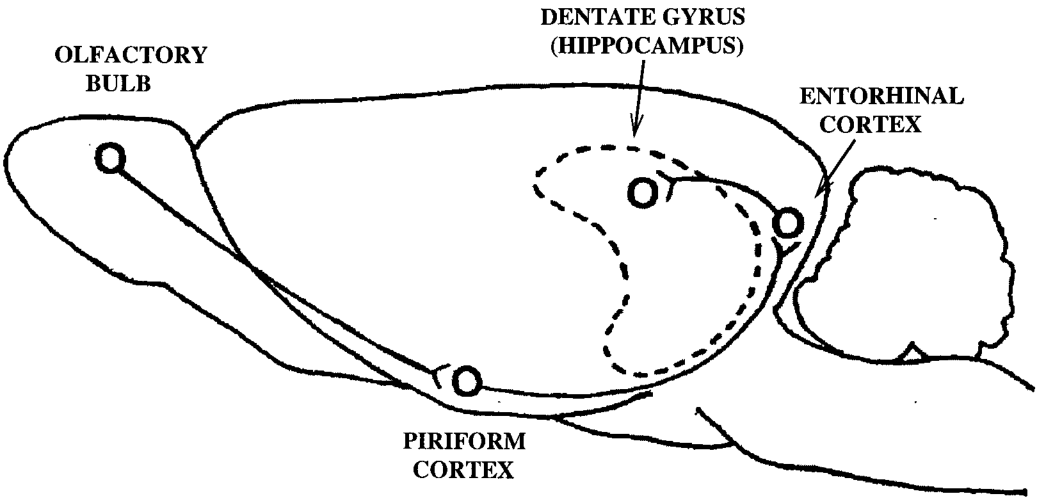

Figure 2.1: The trajectory of the polysynaptic pathway tested in the experiments reported in this thesis. This figure is a highly schematic representation of the rat brain as seen from the side. The olfactory bulb is a brain structure that receives input from olfactory receptors. The information flow runs from olfactory bulb to piriform cortex to entorhinal cortex to the dentate gyrus of the hippocampus (referred to in the thesis simply as the hippocampus). In our experiments, bipolar stimulating electrodes were implanted into the the piriform cortex, bipolar recording electrodes were implanted into the entorhinal and hippocampal dentate gyrus.

the entorhinal cortex and hippocampus is the theta (4–12 Hz in rat) rhythm. The theta activity in these two structures is highly coherent, so that the theta rhythm may serve to temporally coordinate neural activity in these sites to enhance the transmission of neural signals from one site to the other.

In the olfactory system, the gamma (35–85 Hz) rhythm is most commonly seen in the spontaneous EEG and in response to olfactory stimuli (Freeman, 1978; Freeman and Schneider, 1982). One function of the gamma oscillatory state is thought to facilitate the transmission of neural signals from one region to another in order to aid in stimulus binding[1] (Bressler, 1990). Beta-frequency (15–35 Hz) activity is also observed in the olfactory bulb and piriform cortex during odor sampling (Bressler, 1984). The beta rhythm may contribute to the transmission of olfactory representations to the hippocampus (Boeijinga and Lopes da Silva, 1989; Vanderwolf, 1992), and recent studies have suggested that beta burst elicited in both the olfactory bulb and hippocampus by certain odors may serve such a role (Vanderwolf, 1992; Heale et al., 1994).

To further explore the role of oscillatory activity in the flow of olfactory signals to the hippocampus, we applied low intensity, rhythmic electrical stimulation to the piriform cortex to mimic the oscillatory activity in the system. Our objective is to determine the frequencies for optimal signal transmission from the piriform cortex to the hippocampus via the entorhinal cortex.

2.4 EEG Analysis

EEG is never fully deterministic. Therefore, it is usually treated as a random or stochastic process. It should be stressed that the biophysical process underlying

---

[1] stimulus binding: the linking of individual neural representations of different, local features of external stimuli by a common oscillatory pattern of discharge

EEG generation is not necessarily random in nature. It may have such a high degree of complexity that only a stochastic approach is justified.

EEG mainly contains frequency-related activities. Hence, the most common analysis is frequency analysis for which both parametric and nonparametric methods have been employed. Parametric methods, which include AR and ARMA models, and Inverse AR filtering, assume the EEG is generated by a specific model. Nonparametric methods include auto- and cross-correlation, auto- and cross-spectral functions.

The traditional frequency analysis has been widely used to quantify the different oscillatory activities in the EEG (Dumermuth and Molinari, 1987), but the statistical assumptions underlying these methods require the time series to be wide-sense stationary. In reality, the neural processes that generate the EEG are intrinsically dynamic over many time scales, and the EEG can be considered quasistationary only for periods of a few seconds under controlled conditions (Sugimoto et al., 1978). Indeed, it is often the nonstationary nature of the EEG that is of primary interest. Transient changes in the power or peak frequency of EEG rhythms can provide information about the dynamics and reactive properties of neuronal substrates that mediate those rhythms. Unfortunately, these transients are not quantified with traditional frequency analyses that do not include time.

Time-frequency analysis methods, describing the frequency content of a signal as a function of time, are able to quantify these transients. Indeed, these methods have a long history of application to the EEG (Adey et al., 1967; Kawabata, 1973; Gersch, 1987; Gath et al., 1992; Zaveri et al., 1992; Xu et al., 1994; Haykin et al., 1996). One advantage of these techniques is the ability to both quantify changes in EEG activity, and to correlate these changes with experimentally applied stimuli.

In the following chapters, time-frequency analysis of EEG from the entorhinal cortex and the hippocampus will be presented.

Chapter 3

Experimental Set-up

3.1 Animal Preparations

Male Long Evans hooded rats (320–460g) were anaesthetized with 0.9 mg/kg ketamine and 0.05 mg/kg xylazine and were placed in a stereotaxic frame with the skull surface on the horizontal plane. The level of anaesthesia was monitored closely, and 10 to 20% supplemental doses were administered as required. Bipolar, Teflon-coated stainless-steel twisted-wire electrodes (125 μm exposed tips) were implanted in the right piriform cortex (P 3.6 mm, L 6.5 mm, and V 8.5–9.0 mm relative to bregma), medial entorhinal cortex (P 8.8 mm, L5.0 mm, and 0.1 to 0.2 mm above the ventral brain surface), and dentate gyrus of the hippocampus (P 3.5 mm, L2.2 mm, V 4.3 mm) (see Fig. 2.1). One tip of each bipolar electrode was 0.5 mm longer than the other except in the entorhinal cortex where the tip separation was 1.0 mm.

The vertical positions of the stimulating electrodes were adjusted during surgery to minimize current thresholds for field potentials, and recording electrode placements were then adjusted slightly to maximize field potential amplitude. Electrode leads were connected to gold-plated Amphenol pins which were mounted in a 9-pin connector, and the assembly was embedded in dental cement and anchored to the skull with stainless-steel jeweller's screws. One skull screw placed above the contralateral frontal cortex served as a ground and reference electrode. A two week recovery period preceded experimental testing.

3.2 Data Collection

Animals were placed in a 30 x 40 x 30 cm wooden chamber with a Plexiglas front and a wire-grid floor. Data were collected while animals were in a quite, resting state. Animals were habituated to the testing chamber for at least 20 minutes one or two days prior to the start of testing. Electrical stimuli were generated with a Grass S88 stimulator, and photoelectric stimulus isolation units (Grass SIU6B) were used to deliver 0.1 ms biphasic constant-current pulses.

EEG signals were recorded simultaneously from the entorhinal cortex and hippocampus. Bipolar EEG recordings were obtained to eliminate coherence due to activity at the common reference electrode (Fein et al., 1988). EEG was analog filtered (0.3 and 100 Hz) and amplified using a Grass Model 12 Neurodata Acquisition System. Signals were digitized at 256 Hz with a 12-bit A/D board and stored on computer hard disk. EEG was visually screened during acquisition for the presence of movement artifacts.

3.3 Experimental Design

In these experiments we want to determine the frequencies for optimal signal transmission from the piriform cortex to the hippocampus via the entorhinal cortex. Rhythmic stimulation was applied to the piriform cortex and EEG was recorded in both the entorhinal cortex and hippocampus. This procedure enabled tight experimental control over the temporal characteristics of the input signal, and allowed the determination of the frequency response characteristics of both the entorhinal cortex and hippocampus.

Two recording protocols were carried out using similar methods. In a group of 7 animals, 30 s duration samples of EEG were recorded from the entorhinal cortex and hippocampus during stimulation of the piriform cortex with a pulse-train which was ramped from a frequency of 1 to 40 Hz over a period of 25 s. A total of 10 samples were recorded for each animal.

In an experiment to further test the frequency dependence of the propagation of electrically-induced oscillatory activity (n=8), samples of EEG were recorded from the entorhinal cortex and hippocampus during stimulation of the piriform cortex with constant-frequency trains. In these tests, low-frequency trains were delivered during the middle 10 s of 30 s EEG samples. The stimulation frequencies ranged from 2 to 35 Hz. A total of 15 samples were recorded for each condition.

For both protocols, the stimulation train intensities were set to the threshold for a weak hippocampal response during a 10 Hz piriform cortex train.

3.4 Histology

Animals were deeply anaesthetized with chloral hydrate and perfused through the heart with 0.9% saline followed by 10% formalin. The brains were removed and stored in a solution of 20 % glucose in 10% formalin. Frozen, 40 μm thick coronal sections were placed on gelatin-coated slides, dried, and stained with thionin to verify electrode placements. All electrodes were found within target structures.

Chapter 4

Time-Frequency Analysis

4.1 Time-Frequency Representations

The time-frequency representations, which map a one-dimensional signal into a two-dimensional function of time and frequency, can be divided into two main classes: linear and nonlinear time-frequency representations (Cohen, 1995). The linear methods include the short-time Fourier transform (STFT) and wavelet transform (WT). The nonlinear methods include the Wigner-Ville distribution (WVD), the exponential distribution (ED), and the reduced interference distribution (RID). The STFT and WVD are commonly used time-frequency methods and they were used in this thesis. The advantages and disadvantages of each of these two methods will be discussed briefly in this chapter. More details of these two methods and other time-frequency methods can be found in some excellent books and reviews (Cohen, 1989; Boashash, 1991; Hlawatsch and Boudreaux-Bartels, 1992; Cohen, 1995).

4.1.1 The Short-Time Fourier Transform (STFT)

The Fourier transform $X(f)$ of a signal $x(t)$ is defined as

$$X(f) = \int_{-\infty}^{\infty} x(t)e^{-j2\pi ft}dt. \tag{4.1}$$

The Fourier transform of a signal gives the frequency content of the signal. However, it does not provide the time location of the observed frequency component. This limitation is overcome by the STFT.

The STFT is a natural extension of the ordinary Fourier transform. It localizes the frequency components in time by sliding a window $h(t)$ along the signal $x(t)$ and then taking the Fourier transform as shown below (Cohen, 1989; Hlawatsch and Boudreaux-Bartels, 1992; Cohen, 1995)

$$X(t,f) = \int_{-\infty}^{\infty} x(\tau)h(t-\tau)e^{-j2\pi f\tau}d\tau. \tag{4.2}$$

By moving the window $h(t)$, this process maps the signal into a two-dimensional function in a time-frequency plane. The squared magnitude of the STFT is called the spectrogram.

The main advantage of the STFT method is its ease of implementation. It is the most efficient method in computation of time-frequency distributions. Furthermore, the STFT is a linear signal decomposition and there are no cross-terms between the multiple signal components. The major drawback inherent in this method is the tradeoff between time and frequency resolution, that is, the time and frequency resolution cannot be made better simultaneously.

4.1.2 The Wigner-Ville Distribution (WVD)

The WVD of signal $x(t)$ is defined as (Boashash, 1991)

$$W_x(t,f) = \int_{-\infty}^{\infty} z(t+\tau/2)z^*(t-\tau/2)e^{-j2\pi f\tau}d\tau, \tag{4.3}$$

where $z(t)$ represents the analytical signal associated with $x(t)$ and the superscript asterisk (*) denotes complex conjugation. The reason for using the analytical signal is to avoid the cross-terms between positive and negative frequencies and the need for over sampling, as would be required for the real signal (Boashash, 1991).

The WVD yields high resolution in both time and frequency. However, it suffers from two serious shortcomings: (1) the generation of cross-terms (or interference) due to the presence of multiple components in the signal, and (2) the presence of "negative" values that prevents it from being strictly interpreted as an energy distribution.

4.2 The Time-Frequency Coherence

Coherence is a measure of the consistency of phase-relationship between two time series (Marple, 1987). For stationary processes, coherence is defined as the squared magnitude of the complex average of multiple cross-spectra, normalized to the power in each of the two signals. It provides a frequency-specific measure of the phase coupling between two signals and has been applied to the EEG in a number of clinical and experimental contexts (Shaw, 1984; Boeijinga and Lopes da Silva, 1989).

We extended the STFT to the computation of a time-frequency coherence function (Xu et al., 1994). Let $X^{(n)}(t,f)$ and $Y^{(n)}(t,f)$ denote the STFT's of the signals $x^{(n)}(t)$ and $y^{(n)}(t)$, respectively. The superscript (n) denotes the nth realization (sweep) of the two signals. The time-frequency coherence function between the signals $x(t)$ and $y(t)$ is defined as follows:

$$\Gamma_{xy}^2(t,f) = \frac{\left|\sum_{n=1}^{N} X^{(n)}(t,f)Y^{*(n)}(t,f)\right|^2}{\sum_{n=1}^{N}\left|X^{(n)}(t,f)\right|^2 \sum_{n=1}^{N}\left|Y^{(n)}(t,f)\right|^2}, \tag{4.4}$$

where N is the number of sweeps of the $x(t)$ and $y(t)$. Note that t refers to the time coordinate relative to the start of each sweep. Note also that for a fixed t, the time-frequency coherence function $\Gamma^2_{xy}(t, f)$ reduces to the ordinary coherence function.

The time-frequency coherence function is used to measure the efficacy of the transmission of oscillatory signals from the entorhinal cortex to the hippocampus.

4.3 Experimental Results

4.3.1 The Detection of Nonstationarities in EEG Signal

We applied the STFT and WVD to the characterization of two different nonstationary EEG data sets. First, we collected samples of 8–10 Hz spindle discharges, which are obvious *spontaneous* transient events in the cortical EEG. Second, we experimentally imposed nonstationarities into the entorhinal cortex EEG by applying low-intensity stimulation trains to the piriform cortex (first protocol in Section 3.3). Fig. 4.1 shows examples of both types of EEG trace and the results of two different types of time-frequency analysis. As can be seen, the nonstationarities are well delineated by using these procedures. There are some striking differences between the STFT and the WVD images[1,2]: (1) the WVD exhibits a higher resolution than the STFT, both in time and frequency, and (2) the presence of the cross-terms in the WVD makes its interpretation more difficult (particularly for the spindle waves-Fig. 4.1).

We also experimented with the pseudo-WVD, a windowed WVD, which has the effect of suppressing the cross-terms of the WVD (Boashash, 1991; Cohen, 1995).

---

[1] In the STFT displays presented in Fig. 4.1, darkness is a measure of the magnitude of the STFT. In the WVD displays, darkness is a measure of the square root of the WVD. The reason for using amplitude, rather than power, as the z coordinate was merely for providing a better contrast. Same conventions are used in other time-frequency images.

[2] Besides the differences mentioned in the text, there is also a big difference in computation time for calculating the STFT and WVD. For 30 s EEG signal (Fig. 4.1, right), it took only about 15 s to get the STFT result, but 30 minutes to get WVD result. The programs were written in Matlab and run on SUN SPARCstation 10.

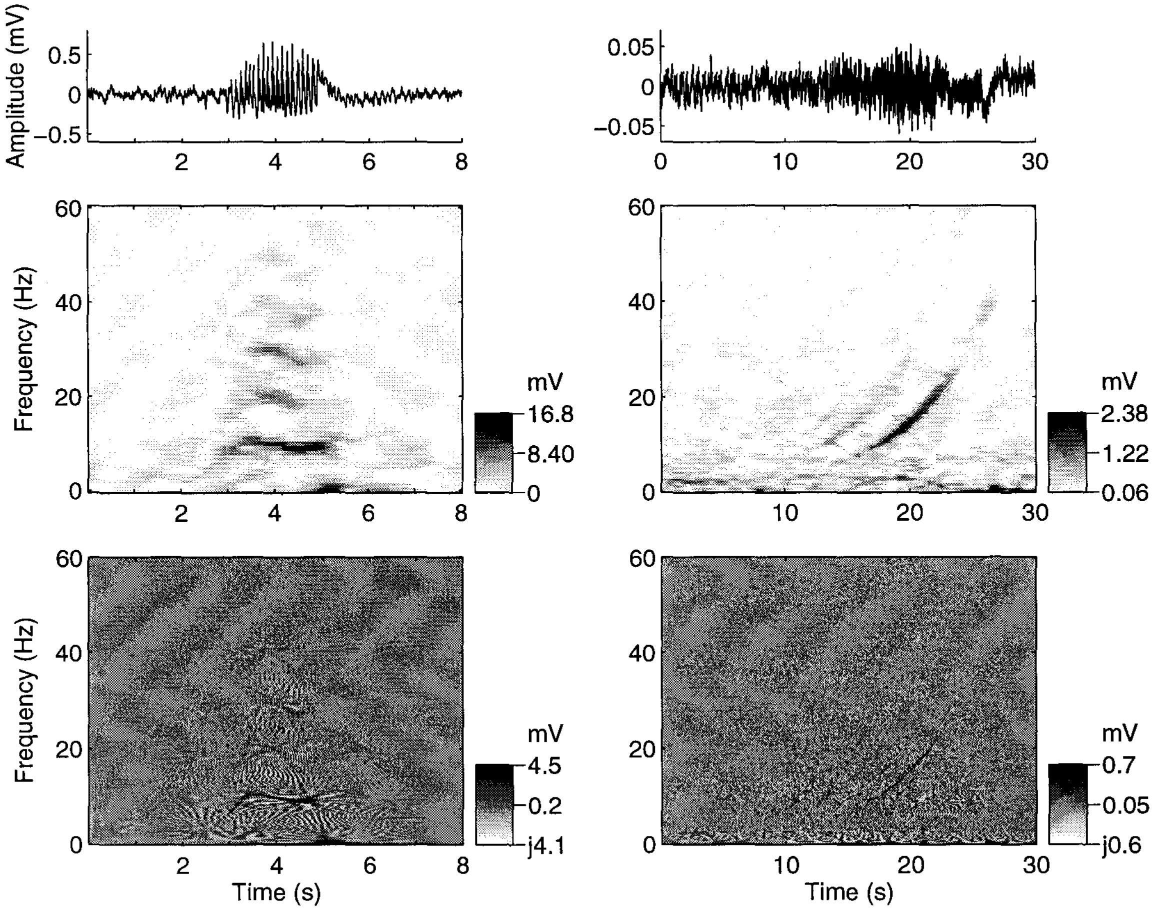

Figure 4.1: Nonstationary EEG samples and their time-frequency representations. The spindle discharge in the upper left panel was recorded from the rat frontal cortex. It is a typical example of a nonstationarity in the *spontaneous* EEG. The EEG trace in upper right panel shows a rather extreme form of nonstationarity, though of much lower amplitude, that is induced in the entorhinal cortex by stimulation of the piriform cortex. The stimulation consisted of a train of pulses that was ramped from 1 to 40 Hz. The middle panels show the results of STFT analysis of these EEG segments. The lower images show the results of standard WVD analysis.

Hanning and Gaussian windows were used to perform the pseudo-WVD. The results were very similar to those obtained by using the standard WVD, except for certain reduction of cross-terms in some parts of the WVD image.

The STFT was used in all the following experiments.

4.3.2 Frequency-Dependent Transmission of Externally Imposed Signals

The STFT was applied to the EEG from the entorhinal cortex and hippocampus under two stimulation protocols (see Section 3.3). The STFT representations were obtained by using a 2.0 s moving window (Hanning window) with a 1.9 s overlap between consecutive computations. A total of 10–15 sweeps of EEG were used to calculate the time-frequency coherence; these sweeps were disjoint in time.

Typical examples of the raw EEG, STFT representations and time-frequency coherence are shown on Figs. 4.2 and 4.3.

Spontaneous EEG

Power in the spontaneous EEG was concentrated at low frequencies under 20 Hz (Figs. 4.2 and 4.3). Theta frequency activity was evident in both the entorhinal cortex and hippocampus EEG recordings, consistent with normal patterns of EEG activity in these sites (Vanderwolf, 1969). Variations in amplitude at frequencies near 8 Hz in both the entorhinal cortex and hippocampal STFT representations reflect nonstationarities in theta activity (Fig. 4.3).

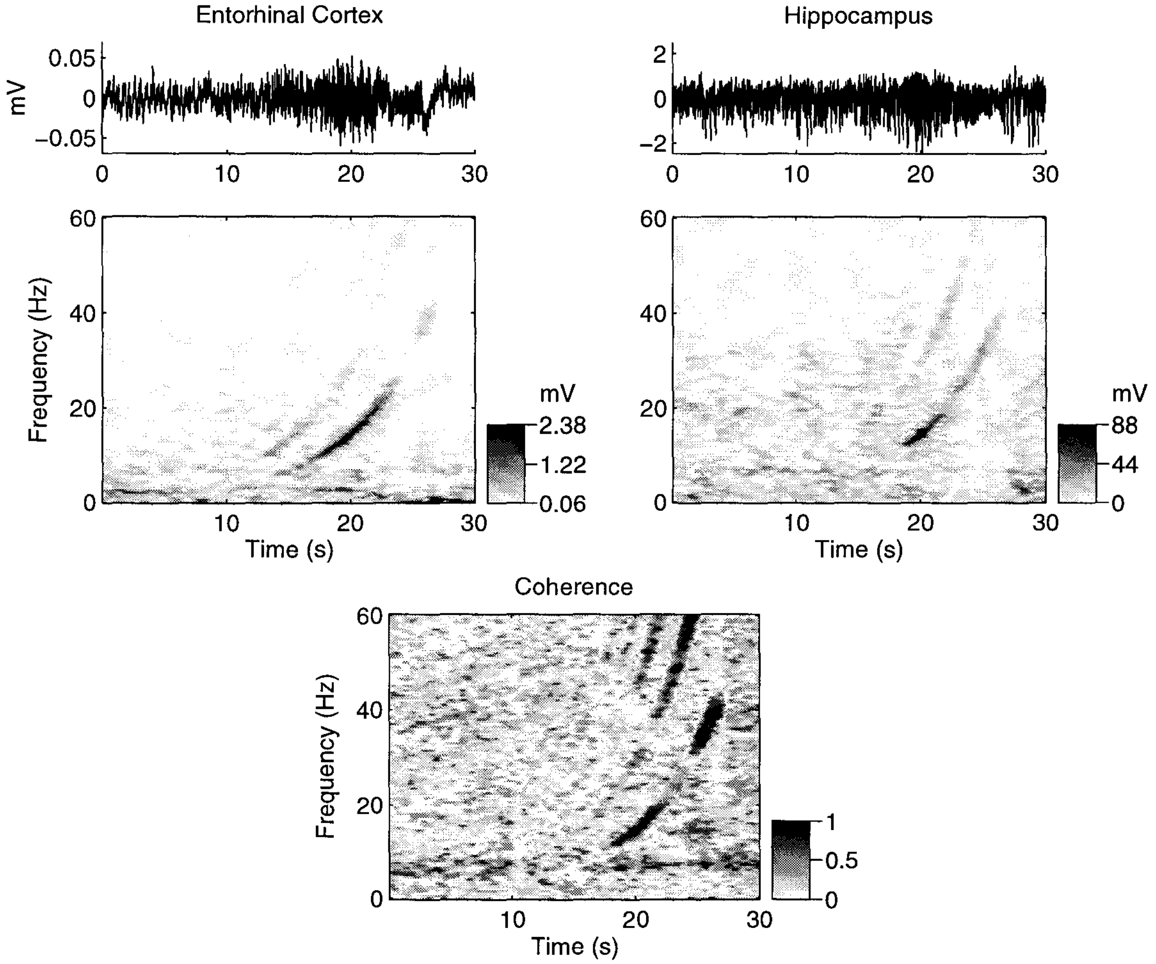

Figure 4.2: Examples of EEG activity in the entorhinal cortex and hippocampus during stimulation of the piriform cortex with a pulse-train which ramped from 1 to 40 Hz. Top panels show the raw EEG, and time-frequency representations of these traces are shown below. Power in both sites evoked by stimulation showed the greatest increase for stimulation frequencies near 17 Hz in this animal. Coherence between the EEG recordings (bottom panel) tended to increase monotonically with stimulation frequency. Upper harmonics, which are only faintly observed in the EEG power, are marked in the coherence measurements.

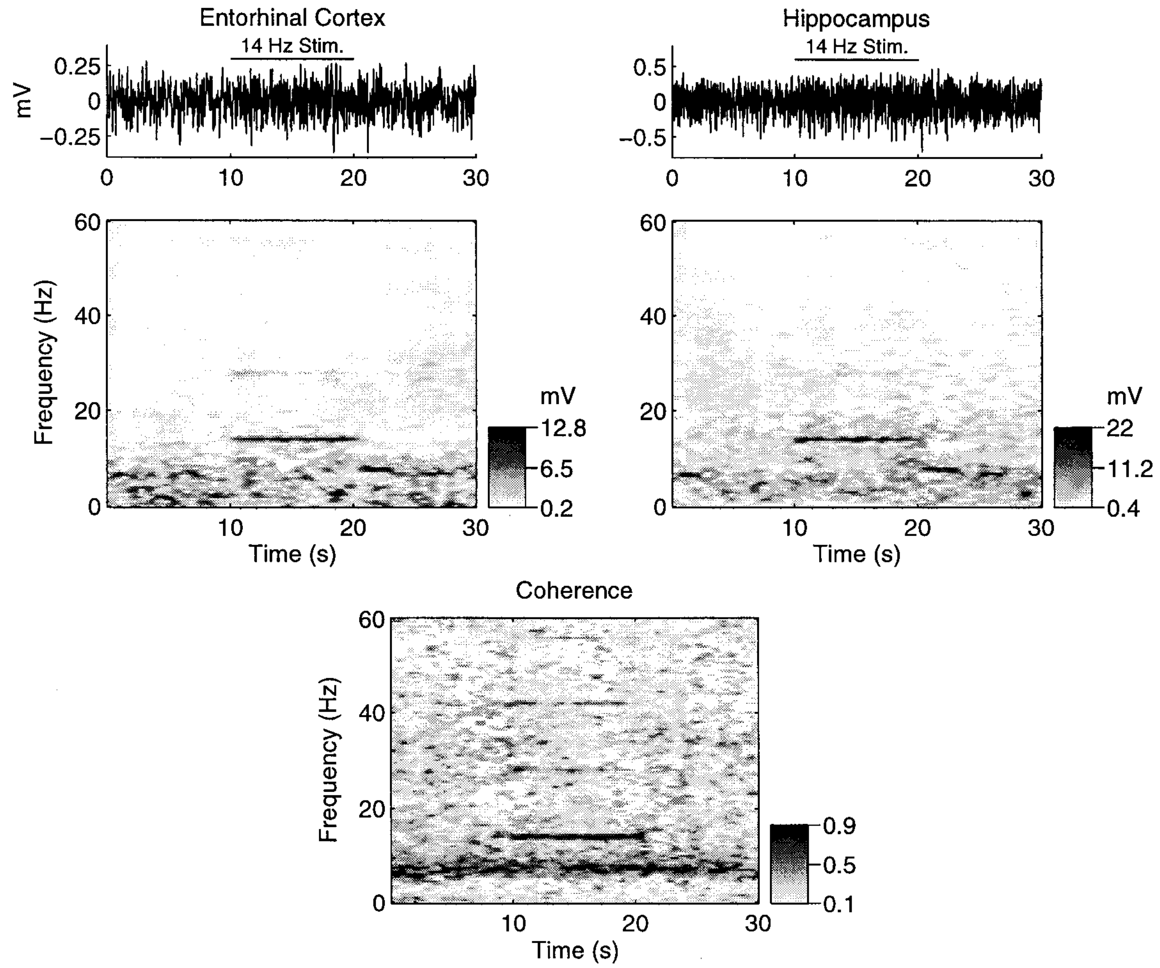

Figure 4.3: Examples of EEG activity in the entorhinal cortex and hippocampus during application of a low intensity, 14 Hz stimulation train to the piriform cortex. Top panels show the raw EEG, and STFT representations are shown below. Coherence between the EEG recordings is shown on bottom panel. Note the enhanced power and coherence at 4–8 Hz (within the theta band) throughout the sweep, and the enhanced power and coherence at the 14 Hz input frequency and its harmonics during the middle 10 s.

Stimulation-Driven EEG

Stimulation-induced responses could seldom be seen in the time-domain above the background noise (Fig. 4.3, upper panels). The effects of the stimulation train, however, are evident in the STFT images (Figs. 4.2 and 4.3). Changes in EEG activity during train delivery were reflected in power spectral peaks in both recording sites at train frequency and its upper harmonics. The amplitude of train-induced spectral peaks changed with the frequency of stimulation. The peak value was found to be near 15 Hz (Fig. 4.2).

Coherence

During spontaneous EEG activity, coherence function was flat except for a peak in the theta band, indicating a consistent phase relationship between EEG activity in the two sites only at this frequency. The time-frequency coherence was strongly affected by train delivery. It showed peaks at the train frequency and its upper harmonics when activities at these frequencies were present at both recording sites (Figs. 4.2 and 4.3).

Frequency Dependence

To determine the effects of stimulation, the total power at the stimulation frequency and its upper harmonics during the *spontaneous* EEG was subtracted from the measures during train delivery. For the coherence measures, the mean coherence in spontaneous EEG was subtracted from the coherence measure during evoked EEG. The measures were standardized for each animal to a percent of the maximum train-related value observed. To reduce the estimation variance, we averaged the STFT of the 10–15 sweeps obtained in the same experimental condition. The results that are described next were based on the averaged STFT.

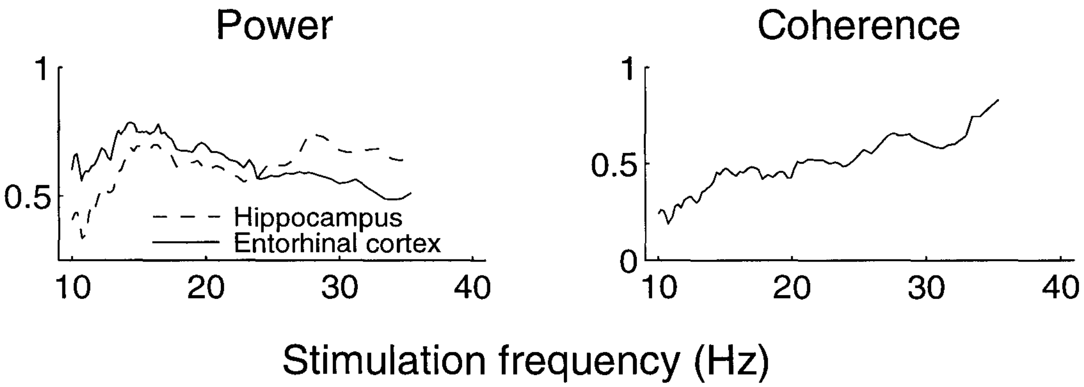

Figure 4.4: Stimulation-related power in the entorhinal cortex and hippocampus and coherence as a function of piriform cortex stimulation frequency—during delivery of ramped frequency trains. Train-evoked power in both site showed similar "tuning curve" and peaked at frequencies near 15 Hz. Hippocampal response showed a secondary peak at about 27 Hz. Coherence increased monotonically with stimulation frequency.

In the experiment when ramped frequency trains were delivered to the piriform cortex, we found that the largest stimulation-dependent increase in power occurred at about 15 Hz in both the entorhinal cortex and hippocampus (Fig. 4.4). There was also a secondary peak in the hippocampus at a mean frequency of 27 Hz. In contrast, the coherence function did not fall off with stimulation frequency; rather it increased monotonically (Fig. 4.4).

When low-intensity, 10 s fixed frequency trains were applied to the piriform cortex, the largest entorhinal cortex and hippocampal EEG responses were evoked at frequencies between 12 and 16 Hz (Fig. 4.5). Stimulation-related coherence values increased monotonically with stimulation frequency upto 35 Hz. Both the responsiveness of the entorhinal cortex and hippocampus to 12–16 Hz stimulation, and the increase in coherence with train frequency, were consistent with the results observed during delivery of ramped frequency trains.

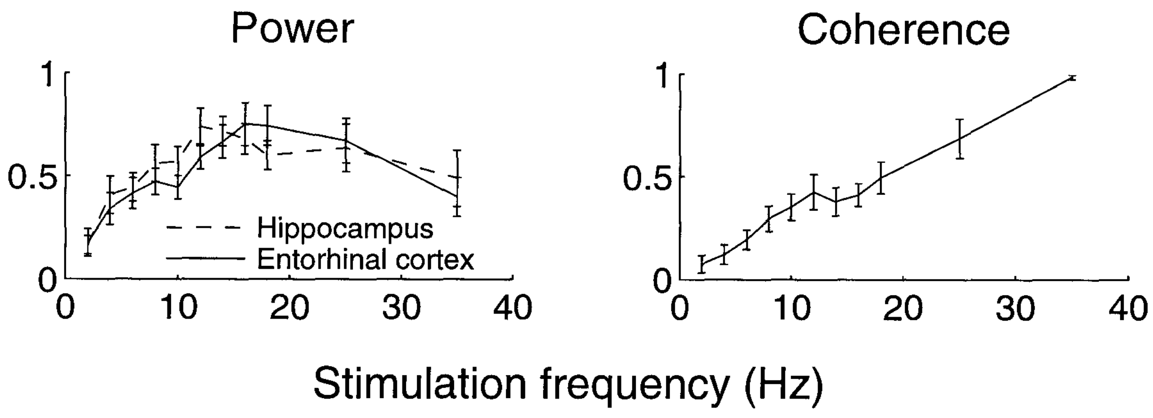

Figure 4.5: Stimulation-related power in the entorhinal cortex and hippocampus and coherence as a function of piriform cortex stimulation frequency—during delivery of fixed-frequency trains. The "tuning curves" for the train-evoked power in the entorhinal cortex and hippocampus were similar, and peaked at frequencies between 12 and 16 Hz. Coherence values were not reduced at higher stimulation frequencies.

4.3.3 Postmortem Testing

To assure that the electrically initiated signals transmitted to the hippocampus was *synaptically* generated within the entorhinal cortex, postmortem recordings were obtained. EEG was recorded from the entorhinal cortex and the hippocampus 5 minutes after death from anaesthesia, while stimulation trains were applied to the piriform cortex. As shown in Fig. 4.6, the electrical artifacts from the stimulation trains were small and well-filtered.

4.4 Discussion

Time-frequency signal processing techniques provide an effective tool for observing the time course of changes in oscillatory states in EEG activity. The time-frequency coherence method has allowed the investigation of the temporal relationship between

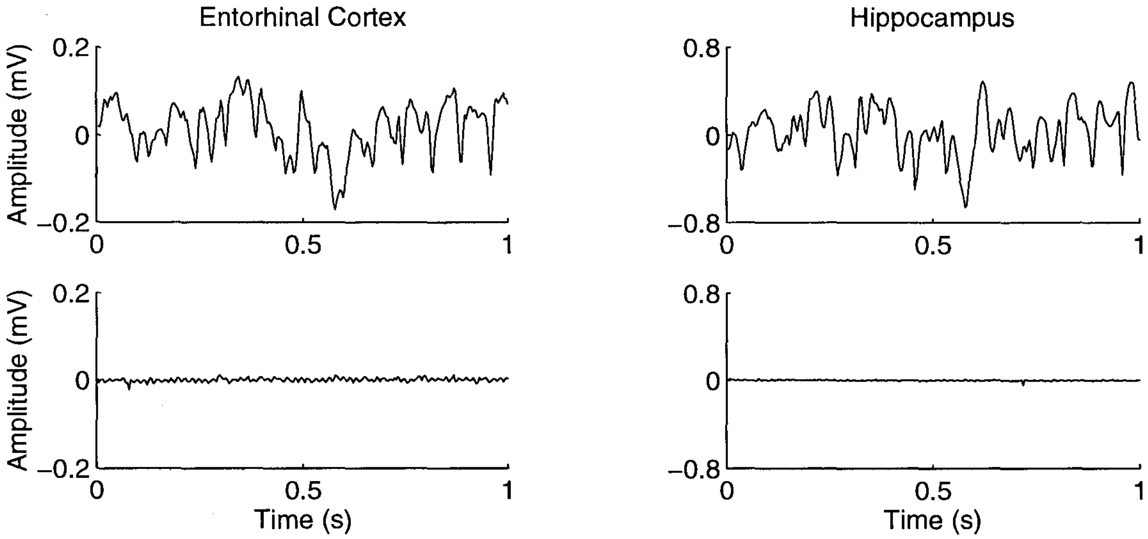

Figure 4.6: Representative EEG traces recorded during experimental tests (the animal is alive) from the entorhinal cortex and hippocampus are shown in upper panels. EEG's recorded from the same sites 5 minutes after death from anesthesia are shown in the bottom panels. A 14 Hz stimulation train was applied to the piriform cortex in both cases. As can be seen, the electrical artifacts from the stimulation trains are minimal.

rhythmic activities in different regions of the brain. These methods provide additional tools for investigating the role that oscillatory states play in determining the flow of neuronal activity from one brain site to another.

4.4.1 Stimulation-Evoked Responses

The methods and results presented here demonstrate that computationally straitforward analytical techniques can be used to quantify the frequency tuning or preferred frequencies of neural transmission between brain sites. These results indicate that signal transmission from the piriform cortex via the entorhinal cortex to the hippocampus is optimal for frequencies of neural activity near 15 Hz. It suggests that the understanding of temporal neural information processing in other brain pathways can be effectively explored by applying similar time-frequency analysis.

Increases in power and coherence in EEG activity in entorhinal cortex and hippocampus at stimulation related frequencies were induced during stimulation of the piriform cortex. Changes in the EEG were more apparent in the time-frequency plane than in the time domain alone, particularly for low frequencies of stimulation. This clearly shows the power of the time-frequency analysis. The time-frequency analysis also resulted in a more dynamic description of the changes in power and coherence of both spontaneous and train-driven EEG activities.

Background rhythms in olfactory cortex often peak around 40 Hz. Therefore it was surprising to find peaks in the power occurring around 15 Hz. It has been reported recently that certain odors do, in fact, trigger responses in this frequency range in the olfactory cortex and hippocampus (Vanderwolf, 1992; Heale et al., 1994). It has been concluded that these odors are activating systems that are tuned to respond to predator signals. This finding, together with our results, suggests that frequency near 15 Hz effectively transmit efferent activity between sites in the olfactory system, and points to a role for rhythmic activity near 15 Hz in the gating of sensory input to the hippocampus via the entorhinal cortex (Heale et al., 1994; Chapman and Racine, 1997; Chapman et al., 1997).

Coherence has previously been reported as a measure of temporal coupling of dominant rhythms in the EEG across multiple sites in the brain (Boeijinga and Lopes da Silva, 1989). Spectral activity in the entorhinal cortex and hippocampus was coherent at the stimulation frequency and its upper harmonics (necessary for complete description of non-sinusoidal activity at the stimulation frequency). These peaks in coherence result from the consistent temporal relationships between train-induced EEG activity in both entorhinal cortex and hippocampus. While the stimulation-induced responses in the entorhinal cortex and hippocampus were tuned at 15 Hz, the coherence function increased monotonically. This indicates although the neural signals above 15 Hz were reduced in magnitude, their phase coupling was even more consistent.

The temporal characteristics of neuronal activity in the system studied here can be further explored by artificial neural network modelling techniques to understand the underlying neural mechanisms. The EEG signals and results obtained here can be used to train or validate the artificial neural network models.

4.4.2 Time-Frequency Analysis

Both the STFT and WVD have been used in this study and their advantages and disadvantages may be drawn from Fig. 4.1.

EEG time series usually contain multiple frequency components. The cross-terms of WVD due to these multicomponent co-exist with real components and make it hard to interpret the WVD result. This drawback limited direct use of the WVD in EEG analysis. Recently, a new class of time-frequency distributions called the reduced interference distribution (RID) has been proposed (Choi and Williams, 1989; Jeong and Williams, 1992). The RID could be regarded as "smoothed" WVD. It provides high resolution in time and frequency while suppressing cross-terms. It has been applied to the tracking of rapid dynamic changes in temporal lobe epilepsy with good results (Zaveri et al., 1992).

There are certain limitations to RID also. The RID, like the WVD, is not a non-negative distribution. This drawback prevents it from being strictly interpreted as an energy distribution. Further, with negative values in time-frequency distribution, it would be impossible to build time-frequency coherence functions whose values are between 0 and 1.

For the applications in this thesis, the WVD and RID have another disadvantage. The WVD and RID do not weight signal evenly across time for a signal with a finite time interval. They weight the middle part of a signal the most when the whole series enter the calculation, and the weights decay toward the beginning and end parts of the series. Hence they are not appropriate for monitoring the magnitude change of stimulation-induced responses, especially when the stimulation frequency ramps from 1 to 40 Hz. On the contrary, the STFT treats each segment of a signal equally by sliding the same window through the whole course of the signal.

With high resolution in both time and frequency, the WVD and RID have good applications in signal detection. On some occasions the cross-terms may be of value in revealing weak components (Haykin and Bhattacharya, 1997). Our primary interest in time-frequency distributions is in their use as a tool for "signal analysis". The features such as positive distribution (its squared magnitude), no cross-terms and good visual presentation possessed by the STFT makes it very appropriate for the studies reported here.

4.4.3 Time-Frequency Representations of Random Processes

As mentioned in Section 2.4, EEG has been treated as a random process. When we estimate power spectrum of a random process, we must consider the bias and variance. The power spectrum estimation of stationary random processes is well established. The periodogram is the classical spectrum estimator. While it is unbiased, it has high variance and usually the variance can be reduced by segmenting the time series and then averaging the individual results.

In this thesis a similar averaging method was used because we were mainly interested in the stimulation-related effects. Multiple realizations (sweeps) of the EEG signal were recorded for the same stimulation condition. The STFT's of these sweeps were then averaged to reduce the estimation variance. The averaged STFT provided a good estimate for stimulation-evoked power in time-frequency plane. However, the nonstationarity in the spontaneous EEG corresponding to individual sweep was not preserved. Therefore, we need a time-varying spectrum estimate with low bias and variance provided that only *one realization* of a non-stationary signal is given. For stationary signals, Thomson developed multiple window method (MWM) to estimate the power spectrum with low bias and variance given a single, short time series (Thomson, 1982). In the next chapter we will introduce multiple window time-frequency analysis, an extension of Thomson's MWM, to estimate the time varying spectrum.

Chapter 5

Multiple Window Time-Frequency Analysis

To date research in time-frequency analysis has been focused on deterministic signals. Only recently, attention has turned to non-stationary random processes (Martin and Flandrin, 1985; Frazer and Boashash, 1994; Bayram, 1996).

To design a time-frequency distribution estimator for a random process, we must consider the bias and variance issues. The conventional time-frequency distribution are typically designed for deterministic signals and to achieve a variety of localization, positivity, cross-term reduction and other goals. Consequently, these designs do not address the bias and variance control issues central to statistical estimator design.

To construct a low bias and variance time varying spectrum estimator, several researchers have extended Thomson's multiple window method to nonstationary signals (Frazer and Boashash, 1994; Bayram, 1996). In the following sections, we will first briefly review Thomson's MWM for stationary signals. Then we will introduce the multiple window time-frequency analysis method and apply it to EEG signals.

We will also compare the performance of multiple window time-frequency analysis by using two sets of window functions.

5.1 Thomson's Multiple Window Method

The classical spectrum estimator for stationary signals is the periodogram. In practice, to reduce the high variance of the periodogram, averaged periodograms are computed. This is done by segmenting the signal, computing a periodogram for each segment, and then averaging the individual results. However, this procedure increases the bias of the spectrum estimate due to the use of a shorter window for each segment. If we have enough data, we may get the power spectrum estimate with desired bias (or frequency resolution) and variance. However, when data length is limited, the tradeoff between bias and variance is inevitable.

For short, time limited signals, Thomson suggested using a different set of windows to compute several periodograms of the *entire signal* and then averaging the resulting periodograms to construct a spectrum estimate (Thomson, 1982). To get an estimate with low bias and low variance, the windows must be, (1) optimally concentrated in frequency (to minimize bias), and (2) mutually orthogonal (to minimize variance). The optimum windows satisfying these requirements for signals with finite length are Slepian sequences or discrete prolate spheroidal sequences.

5.1.1 Slepian Sequences

The Slepian sequences are the eigenvectors of the Toeplitz eigenvalue equation (Slepian, 1978)

$$\sum_{m=0}^{N-1} \frac{\sin 2\pi W(n-m)}{\pi(n-m)} \nu_m^{(k)}(N,W) = \lambda(N,W)\nu_n^{(k)}(N,W) \qquad (5.1)$$

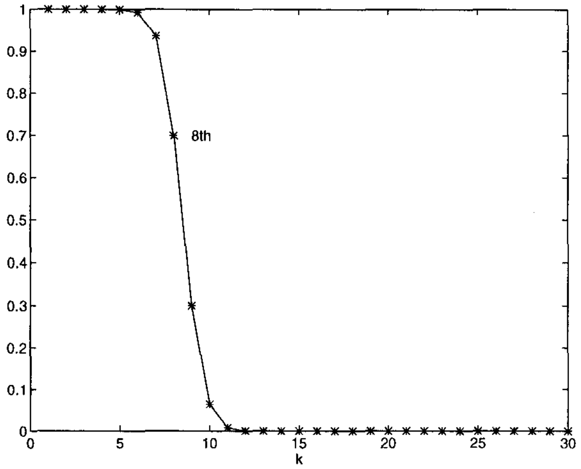

Figure 5.1: Eigenvalues for the case N=256 and NW=4. As we can see the first 8 eigenvalues are very close to 1 corresponding to the first $K = 2NW = 8$ windows that have a negligible effect on the bias of the spectrum estimator.

where N is the length of the eigenvectors (or data), and W is a half-bandwidth that defines a small local frequency band centered around frequency f: $|f - f'| \leq W$. Equation (5.1) derived from the operation of a time-limitation followed by band-limitation of the signal (Slepian, 1978). Therefore, the Slepian sequences are the orthogonal time-limited functions most concentrated in the frequency band $[-W, W]$.

The Slepian sequences are ordered by their eigenvalues:

$$1 > \lambda_0 > \lambda_1 > \ldots > \lambda_{(N-1)} > 0.$$

The eigenvalue, λ_k, gives the fraction of energy within the band $[-W, W]$. The first $2NW$ eigenvalues are very close to 1 (Fig. 5.1), indicating that the spectra of these lower-order Slepian sequences have large energy concentration within the local frequency band $[-W, W]$. Fig. 5.2 shows an example of the Slepian sequences and their Fourier transform.

As shown in Fig. 5.2, the data windows have different shapes and weight the

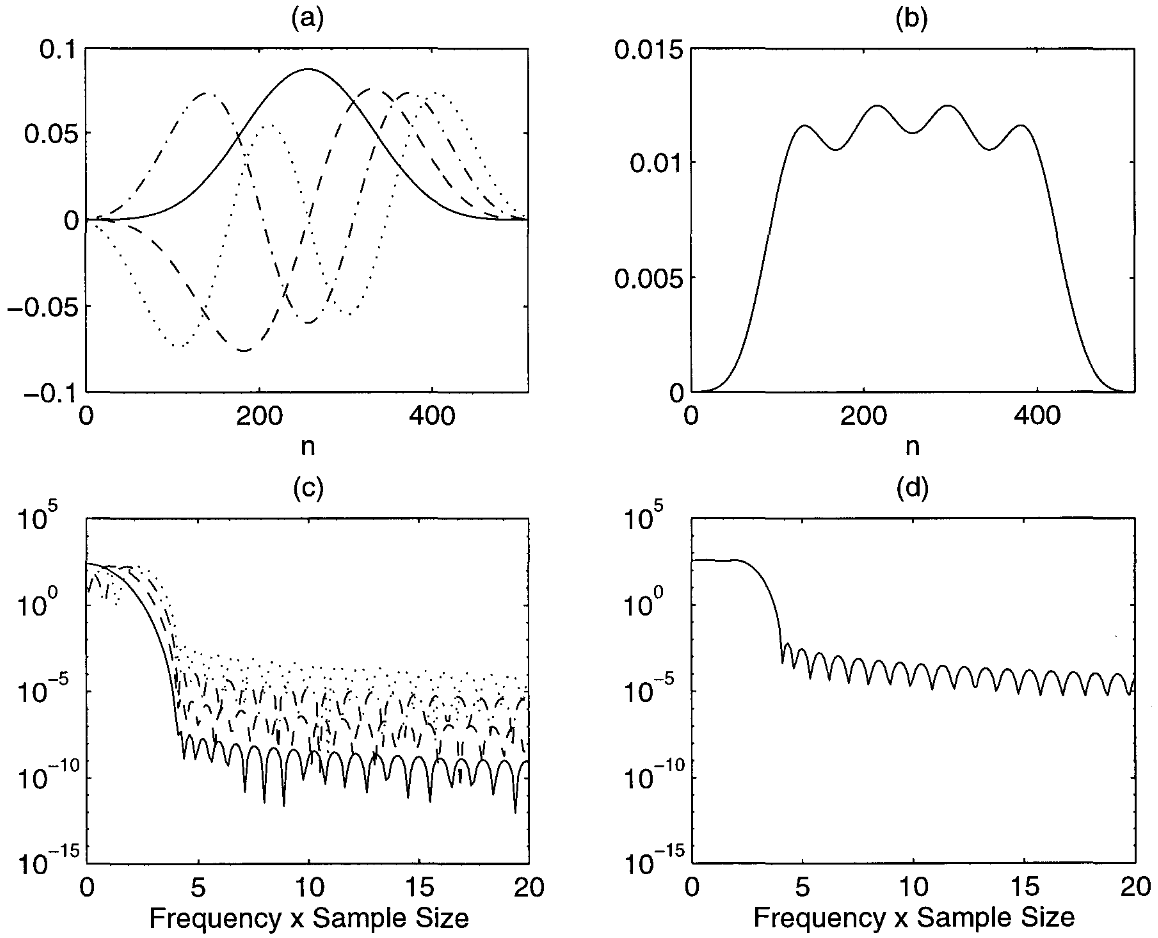

Figure 5.2: The first 4 Slepian sequences and their Fourier transform for the case N=512 and NW=4. (a) the first 4 individual sequences. (b) the sum of magnitude square of the 1st 4 sequences. (c) complex amplitude square of the Fourier transform of the Slepian sequences in (a), (d) the sum of individual forms in (c). As we can seen, the combination of the 4 windows covers more data samples than a single bell-shaped window. In (a) and (c), 0-order: solid line; 1st-order: dashed line; 2nd-order: dash-dotted line; 3rd-order: dotted line.

signal differently. A combination of these windows in the MWM therefore provides a more uniform weighting to different parts of the record (Fig. 5.2, a, b). This leads to a smaller variance of the spectral estimate than with the use of a single conventional bell-shaped window. In Thomson's MWM, only the first few Slepian sequences with their eigenvalues close to 1 are used. Hence the signal power concentration within the analysis band $[-W, W]$ is large. This concentration property results in a low bias estimate of the spectrum.

5.1.2 MWM Outlines

Steps to compute the spectral estimate of $x(n)$, $(n = 0, 1, \dots, N-1)$ using Thomson's MWM are as follows:

1. Specify N and W, where N is the number of data point, and W depends on the desired time-bandwidth NW (or frequency resolution).
2. Use (5.1) to compute[1] λ_k's and ν_k's; actually the first $K = 2NW$ terms with the largest eigenvalues are needed[2].
3. Apply ν_k to the entire length-N data $x(n)$ and take DFT to get kth spectrum estimate $x_k(f)$ as shown below:
$$x_k(f) = \sum_{n=0}^{N-1} x(n)\nu_n^k e^{-j2\pi fn}. \tag{5.2}$$
We call $x_k(f)$ the kth eigencoefficient and $|x_k(f)|^2$ the kth eigenspectrum.
4. Average K eigenspectra to get an estimate of the spectrum as shown below
$$\hat{S}(f) = \frac{1}{K}\sum_{k=0}^{K-1}\frac{1}{\lambda_k}|x_k(f)|^2. \tag{5.3}$$

---

[1] The calculation do not need to be repeated every time. A database could be built for common N and W and the sequences could be retrieved whenever needed.

[2] Thomson suggested the use of $K = 2NW-1$ to $K = 2NW-3$ to minimize higher order window leakage.

As shown in Fig. 5.1, the first few eigenvalues are very close to one. Equation 5.3 can be simplified to

$$\hat{S}(f) = \frac{1}{K} \sum_{k=0}^{K-1} |x_k(f)|^2 . \tag{5.4}$$

Equation (5.3) is the crude multiple window spectrum estimate. We use only the first few largest K ($K \leq 2NW$) eigenvalues and their corresponding eigenvectors. K controls the tradeoff between bias and variance. Larger K gives smaller variance but larger bias.

While the lower-order eigenspectra have excellent bias properties, there is some degradation as k increases towards 2NW. Thomson also developed an *adaptive* MWM estimate (Thomson, 1982). In the adaptive version, a set of frequency-dependent weights $d_k(f)$, instead of $1/\lambda_k$, is used to downweight the higher-order eigenspectra. The adaptive MWM results in a lower bias at higher frequencies than the crude MWM but it requires more computation. In the applications described below, we used only the very first few eigenspectra ($K \leq 2NW - 3$) and found there was no big difference in both low and high frequencies using the two methods. In the EEG analysis, we used the MWM described in (5.4).

5.1.3 Coherence

Coherence can be obtained from *one realization* of the multichannel data using Thomson's MWM. Given two time series $x(n)$ and $y(n)$, ($n = 0, 1, 2, \ldots, N-1$), their eigencoefficients $x_k(f)$ and $y_k(f)$ can be obtained using (5.2). The estimated coherence is (Thomson, 1982)

$$\gamma_{xy}^2(f) = \frac{\left|\sum_{k=0}^{K-1} x_k(f) y_k^*(f)\right|^2}{\sum_{k=0}^{K-1} |x_k(f)|^2 \sum_{k=0}^{K-1} |y_k(f)|^2}, \tag{5.5}$$

where $K \leq 2NW$ is the number of windows used and the asterisk denotes complex conjugation.

5.2 Multiple Window Estimate of Time-Frequency Distribution

Thomson's MWM has been extended to the time-frequency analysis (TFA) (Frazer and Boashash, 1994; Bayram, 1996). The multiple window(MW) TFA performs in a similar way as the STFT. Instead of applying a single sliding window along the signal, the MW-TFA applies a set of sliding windows and then takes the average:

$$X_{MW}(t,f) = \frac{1}{K} \sum_{k=0}^{k=K-1} |X_k(t,f)|^2, \tag{5.6}$$

where $X_k(t,f)$ is the STFT using the k-th window $h_k(t)$ computed as follows:

$$X_k(t,f) = \int x(\tau) h_k(\tau - t) e^{-j2\pi f\tau} d\tau, \tag{5.7}$$

where $x(t)$ is the signal to be analysed.

The multiple window time-frequency coherence is defined as

$$\Gamma_{MW}(t,f) = \frac{\left|\sum_{k=0}^{K-1} X_k(t,f) Y_k^*(t,f)\right|^2}{\sum_{k=0}^{K-1} |X_k(t,f)|^2 \sum_{k=1}^{K-1} |Y_k(t,f)|^2}. \tag{5.8}$$

Two sets of windows have been used in MW-TFA (Frazer and Boashash, 1994; Bayram, 1996). One of them is the Slepian sequences described previously and the other is called Hermite functions. We will give a brief overview of Hermite functions before we apply MW-TFA to EEG data and give a comparison using these two sets of windows.

5.2.1 Hermite Functions

The Hermite functions are the eigenfunctions of a localization operator over the region (Daubechies, 1988)

$$\{(t,f) : t^2 + f^2 \leq R^2\}. \tag{5.9}$$

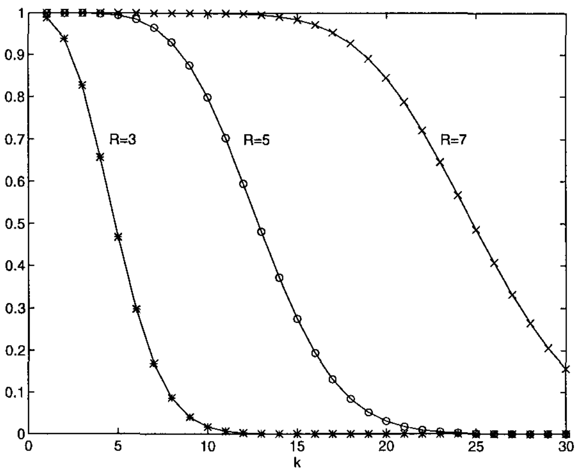

Figure 5.3: Eigenvalues $\lambda_k(R)$, $k = 0, 1, \ldots, 20$ for $R = 3$, $R = 5$, and $R = 7$.

The k-th order Hermite function is defined as,

$$h_k(t) = \pi^{-1/4}(2^k k!)^{-1/2}\left(t - \frac{d}{dt}\right)^k e^{-t^2/2}, \quad k = 0, 1, 2, \cdots. \tag{5.10}$$

The eigenvalues of the localization operator over the region (5.9) are given by

$$\lambda_k(R) = 1 - e^{-R^2/2}\sum_{i=0}^{k}\frac{1}{i!}2^{-i}R^{2i}. \tag{5.11}$$

The Hermite functions are optimally concentrated in the circular time-frequency region (5.9). Similar to Slepian sequences, the eigenvalues λ_k give the fraction of energy within the region (5.9). The closer the k-th eigenvalue is to 1, the better the concentration of the k-th order Hermite function is. Hence, for a given R, there are only a few Hermite functions with good concentration in the region (5.9). Fig. 5.3 shows a plot of $\lambda_k(R)$ for different values of R. The first 4 Hermite functions and their Fourier transforms are shown on Fig. 5.4.

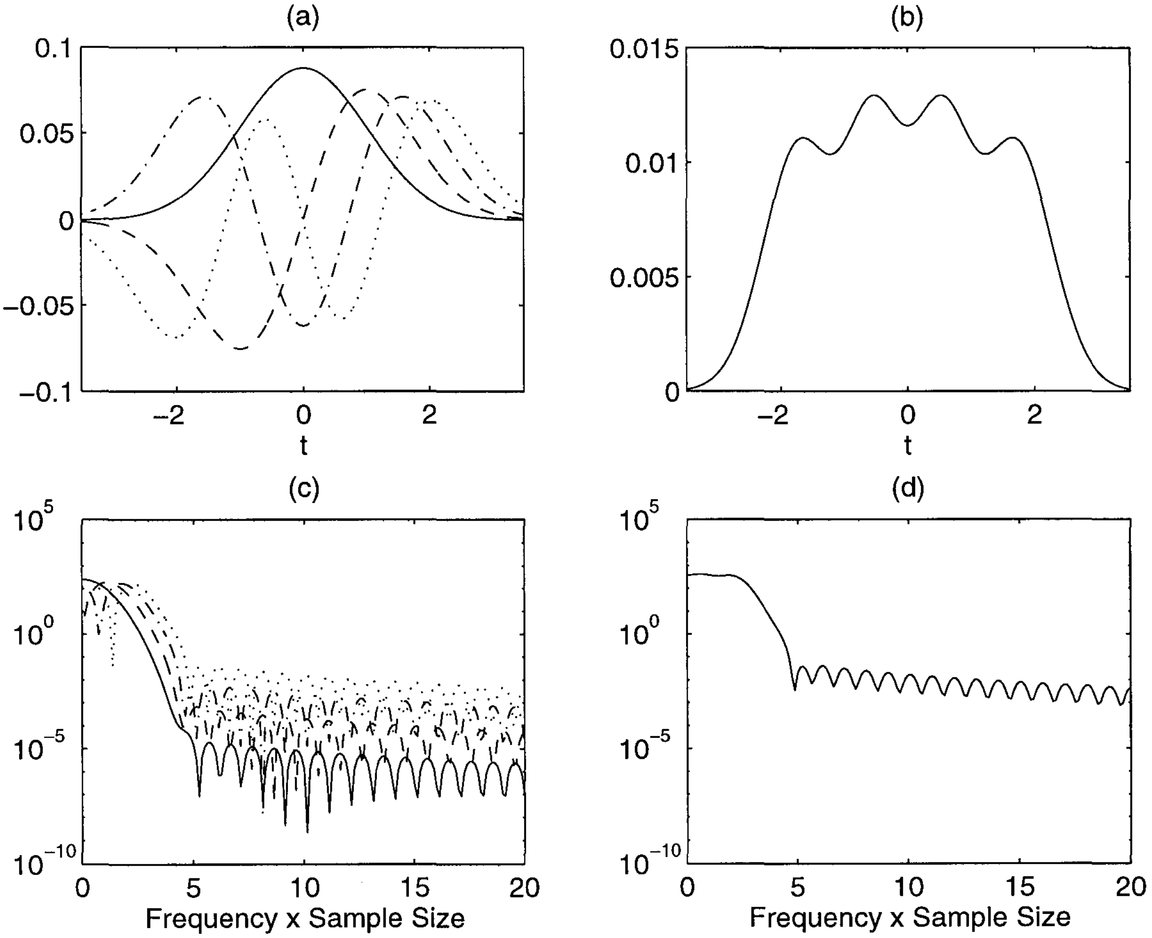

Figure 5.4: The first 4 Hermite functions and their Fourier transform. (a) first 4 Hermite functions. (b) the sum of magnitude square of the 1st 4 sequences. (c) complex amplitude square of the Fourier transform of the Hermite functions in (a), (d) the sum of individual forms in (c). In (a) and (c), 0-order: solid line; 1st-order: dashed line; 2nd-order: dash-dotted line; 3rd-order: dotted line.

5.2.2 MW-TFA of EEG

The MW-TFA was applied to the EEG signals in a similar fashion to that used in the STFT case. The MW time-frequency distribution was obtained by using a set of 2.0 s windows with a 1.9 s overlap between consecutive computations. The multiple window time-frequency coherence was calculated using (5.8). Examples of MW-TFA results are shown in Figs. 5.5 and 5.6

Spontaneous and Train-Driven EEG

The results using MW-TFA shown in Figs. 5.5 and 5.6 are similar to those using the STFT in Figs. 4.2 and 4.3. Both the theta activity and increased activity at stimulation-related frequency and its upper harmonics are evident in MW-TFA images. Fig. 5.5 shows that the stimulation-related power in the entorhinal cortex and hippocampus is peaked near 17 Hz, but the coherence increases monotonically with the stimulation frequency.

The differences of the STFT and MW-TFA images are also apparent. The MW-TFA results in poor resolution in both time and frequency due to wider effective time window and broader frequency bandwidth. The variance of MW-TFA representation is lower than that of STFT image, this being benefited from averaging.

Coherence

One advantage of the MW-TFA is the ability to obtain time-frequency coherence from *one realization* of the data, which is impossible with the STFT. The time-frequency coherence in Fig. 5.6 shows the clear nonstationarity of the coherent activity between the entorhinal cortex and hippocampus in the theta range. The time-frequency coherence in Figs. 4.2 and 4.3 does not show the time correspondence for the spontaneous EEG for individual realizations.

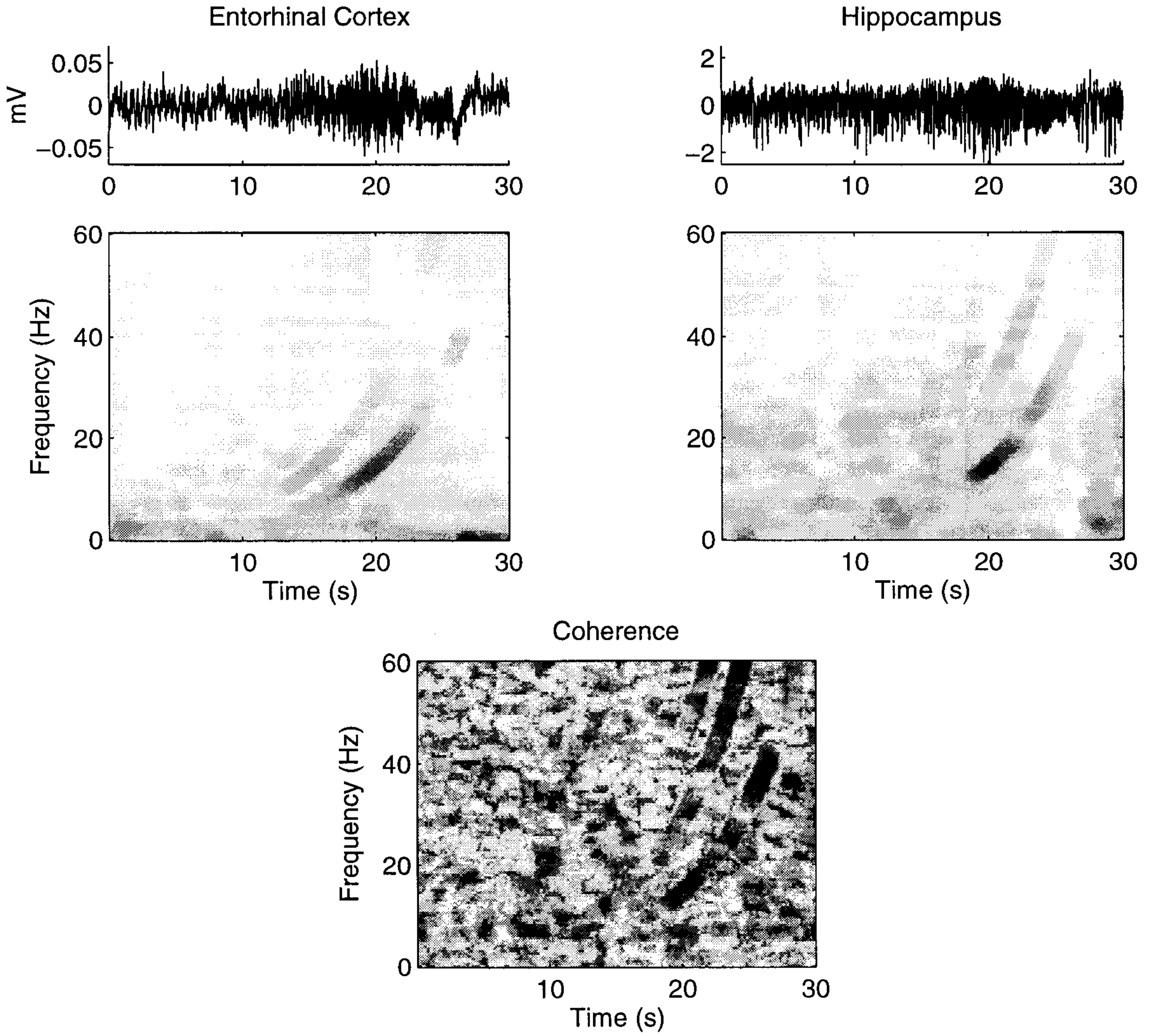

Figure 5.5: Time-frequency representations of EEG's shown in Fig. 4.2 using MW-TFA with Slepian Sequences. Parameters of the sliding windows: $N = 512$, $NW = 4$, $K = 4$.

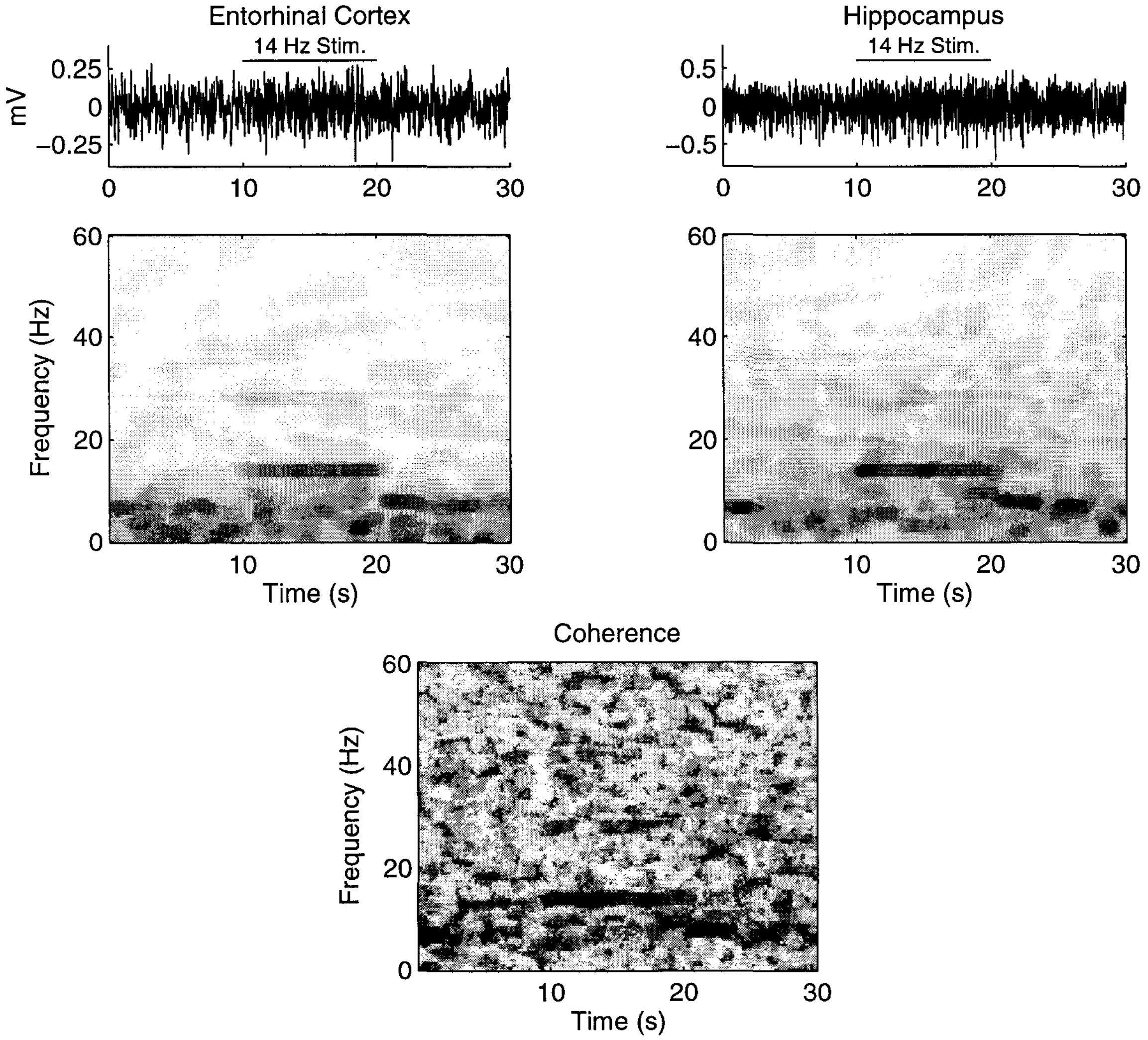

Figure 5.6: Time-frequency representations of EEG's shown in Fig. 4.3 using MW-TFA with Slepian Sequences. Parameters of the sliding windows: $N = 512$, $NW = 4$, $K = 4$. Note high coherence values in theta range only at times when theta activity appears in both the entorhinal cortex and hippocampus.

5.2.3 Comparison Between the Two Window Functions

The shapes of the Slepian sequence and Hermite functions are very similar (Figs. 5.2 and 5.4). To make a fair comparison between the two window functions, the 0-order windows of the two functions were matched with least-mean-squared error in time domain. To achieve a good concentration in time-frequency plane, 4 windows were used in all the cases, except for $NW = 2$ where only 2 windows were used. Figs. 5.7-5.10 show the results.

The well-matched windows differed only slightly in the time domain (Fig. 5.7 and Fig. 5.8, left) for the first four windows. The Hermite windows had higher leakage and wider bandwidth than those of Slepian sequences (Fig. 5.8, right) in the frequency domain. The differences were larger for higher NW values. Both the higher leakage and broader bandwidth will introduce more bias into the estimation. However, the differences of the two functions did not introduce noticeable difference in MW-TFA results (Figs. 5.9 and 5.10).

Selection of Time Window Length

As shown in Fig. 5.8, the actual time windows are shorter and the frequency bandwidth are wider as NW value grows. For piecewise stationary signals, as shown in Fig. 5.10, longer time windows give better frequency resolution and reasonably good time resolution. For highly nonstationary signal, as the one in Fig. 5.9, longer windows work better when the signal varies slowly (around 15 s) and shorter windows has better results when the signal varies fast (around 25 s). It indicates that for signals containing the frequency content varying with time at different rate, it may be necessary to use different window lengths (or sizes) for different parts of the signal.

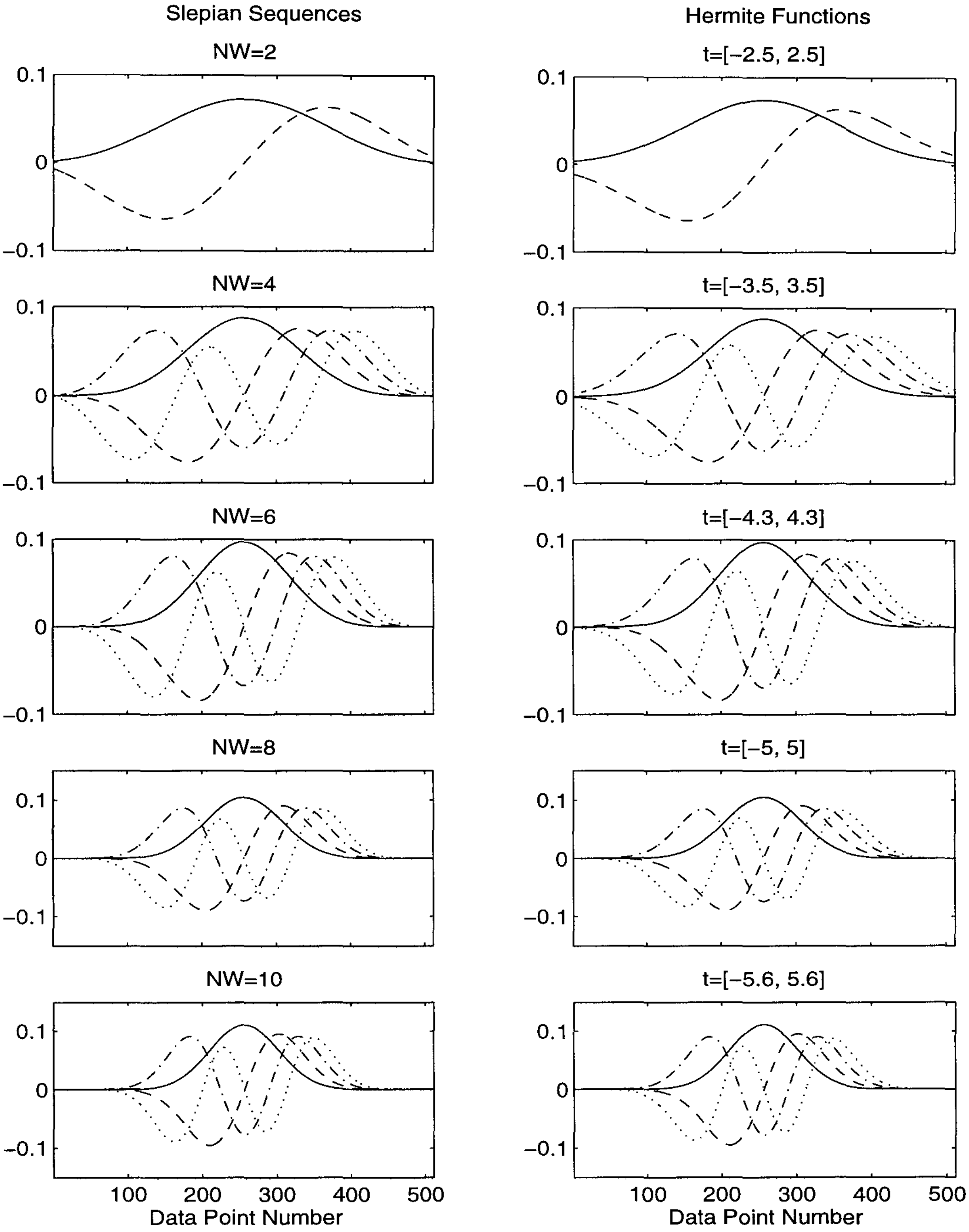

Figure 5.7: The first 2–4 windows for matched Slepian sequences and Hermite functions, for the case of $NW = 2, 4, 6, 8, 10$ and $N = 512$. The value of $t = [-T, T]$ is the range of t in (5.10) to calculate the matching Hermite functions for the Slepian sequences with the corresponding NW . Panels in the same row are matching pairs. 0-order: solid line; 1st-order: dashed line; 2nd-order: dash-dotted line; 3rd-order: dotted line.

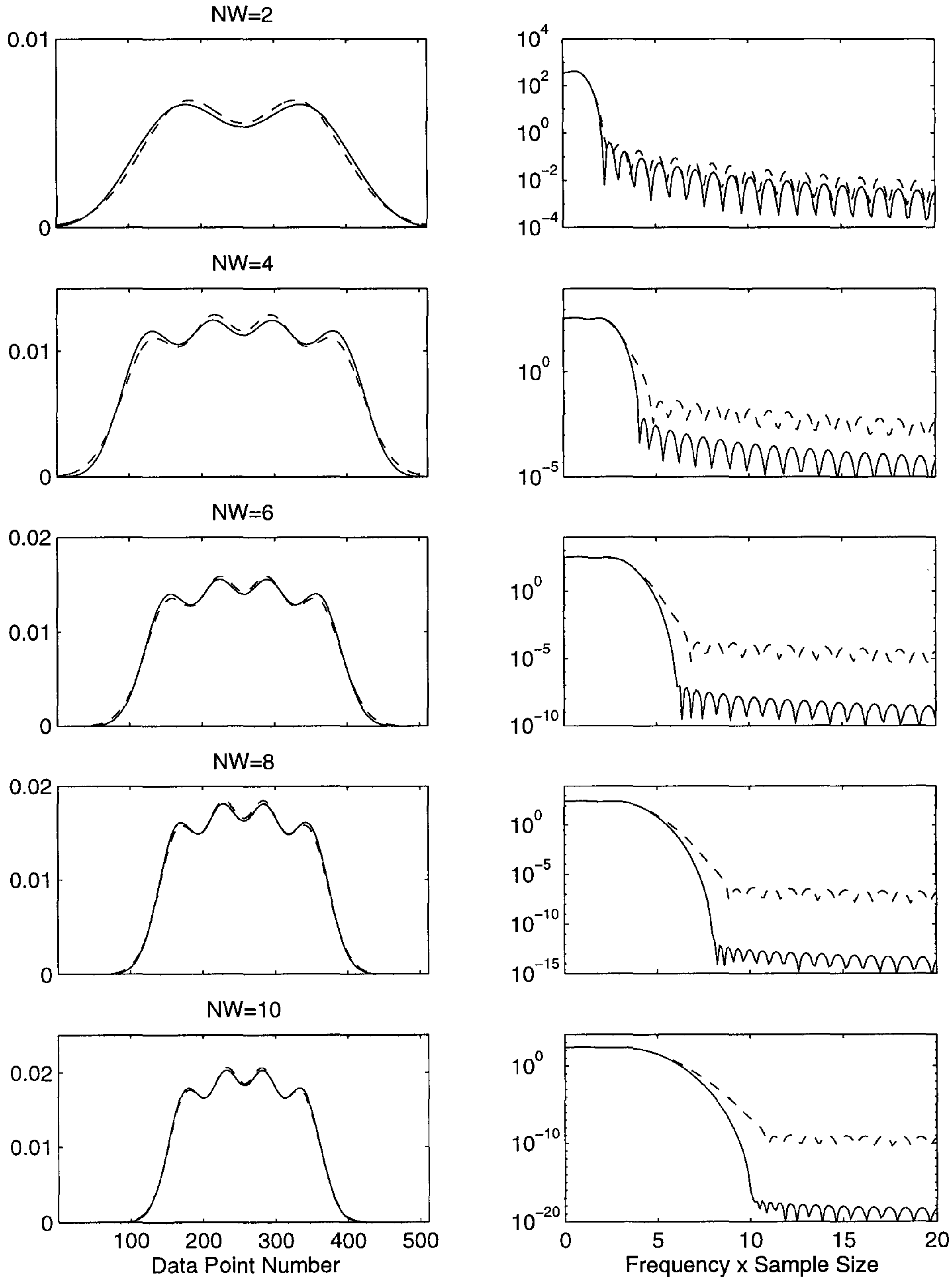

Figure 5.8: Sum of the Slepian sequences (solid) and Hermite functions (dashed) in Fig. 5.7 in time and frequency domain. Left: sum of the magnitude square, Right: sum of the complex magnitude square of their Fourier transforms. Note the broader bandwidth and higher leakage of Hermite windows.

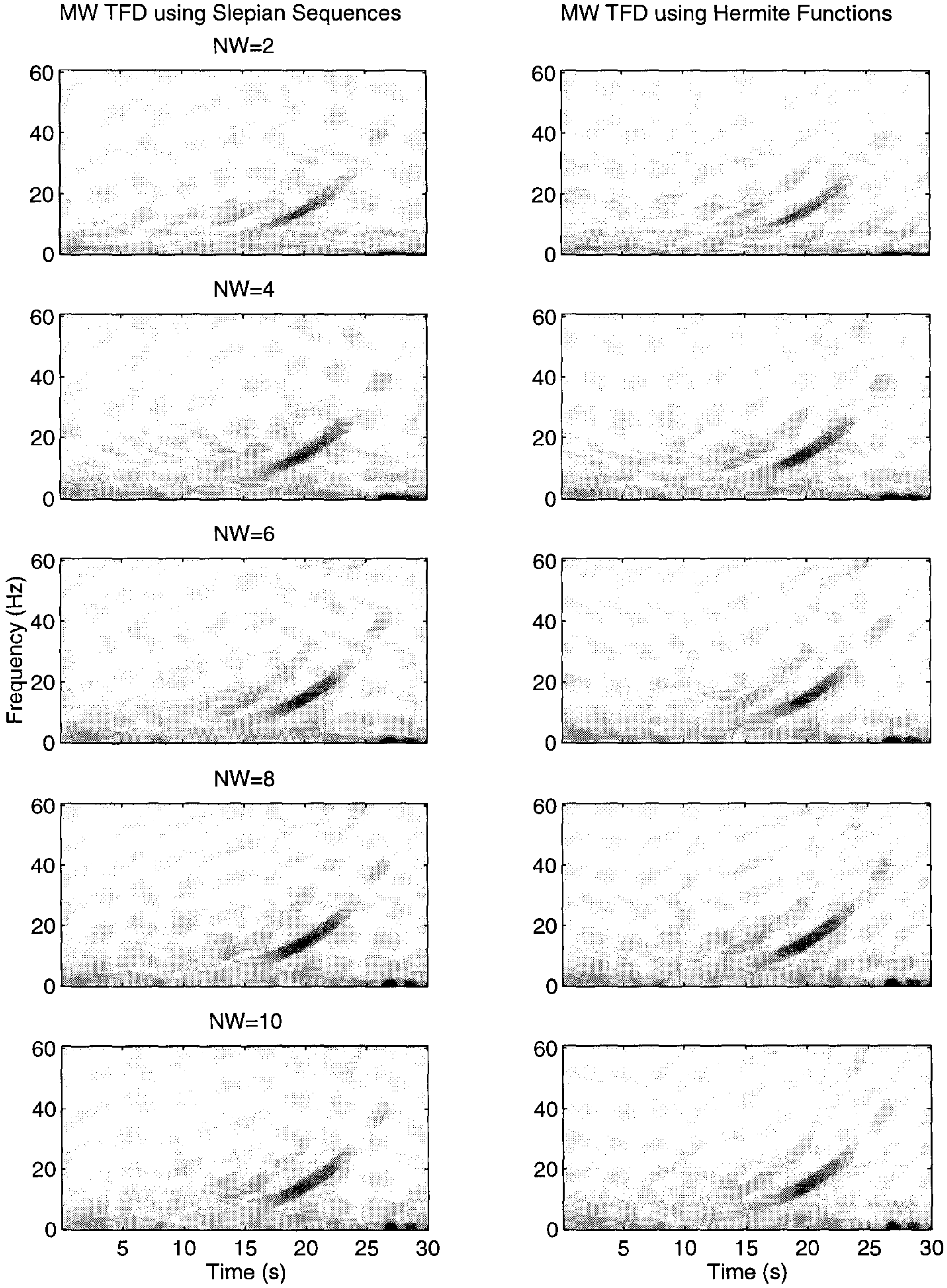

Figure 5.9: Time-frequency representations of MW-TFA using Slepian sequences (left) and Hermite functions (right) of the EEG recorded from the entorhinal cortex shown in Fig. 5.5. Panels in the same row are matching pairs.

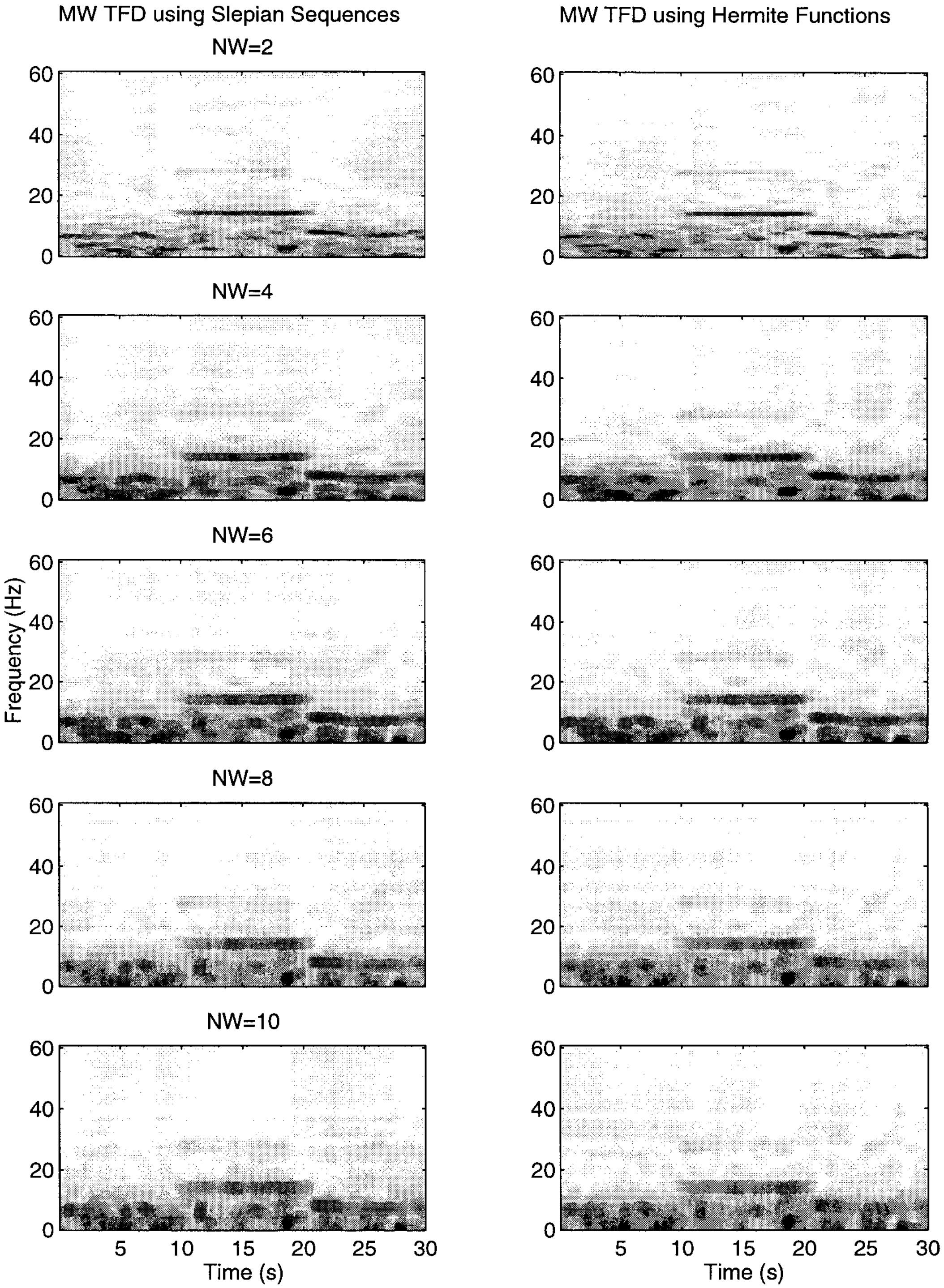

Figure 5.10: Time-frequency representations of MW-TFA using Slepian sequences (left) and Hermite functions (right) of the EEG recorded form the entorhinal cortex shown in Fig. 5.6. Panels in the same row are matching pairs. Note the better time resolution and poorer frequency resolution as *NW* value grows.

5.3 Discussion

5.3.1 MW-TFA and STFT

The MW-TFA provides us a useful tool to estimate the time-frequency distribution with low bias and low variance for a *single realization* of data, which is usually the case for time varying signals. Although the MW-TFA has poorer time and frequency resolutions than those of the STFT, it has a lower variance. This is consistent with the observation made by Frazer and Boashash (1994). The most appealing property of the MW-TFA is that it enables us to estimate the time-frequency coherence from a *single realization.* This provides us an effective tool for investigating the temporal relationship between EEG signals in different brain regions from time to time. To our knowledge, it is the first attempt to extend Thomson's MW coherence to time-frequency coherence.

To study the stimulation-evoked signals in this report, we were able to record more than one realization of the signal under the same condition. The high variance of single STFT was reduced by averaging the STFT's of these realizations without sacrificing the bias (due to the same window length). The averaged STFT could thus provide us a low variance estimate with better time and frequency resolutions than the MW-TFA. The averaged STFT is more suitable for repeatable signals in the current study. For spontaneous EEG which is impossible to obtain multiple realizations, the MW-TFA should be the one to use.

5.3.2 Slepian Sequences and Hermite Functions

We made a fair comparison between these two windows by matching them in terms of having least-mean-squared errors in the time domain. Although there were slight differences in time and frequency domain alone for the first few windows, there were no apparent differences in the time-frequency representations.

The Hermite functions concentrate their energy in the circular region (5.9) in the time-frequency plane. The Hermite functions are independent of R and the R-dependence is completely contained in the eigenvalues. For a given R, the number of Hermite functions which could be used is fixed to achieve a good concentration in the region (5.9). This fixed concentration region is reflected in Fig. 5.8. When using 4 windows, as time range t increases, the increase in frequency band companies with the decrease of the actual time window. Hence, the concentration region in the time-frequency plane is kept the same for windows with different t range. The Slepian sequences concentrate their energy in a rectangular region — $[-T, T]$ x $[-W, W]$ in the time-frequency plane, where $[-T, T]$ is the time limit of the windows (N data points) and $[-W, W]$ is the frequency bandwidth. This rectangular region is maintained when $2NW$ windows are all employed. When we use only fixed number of windows for different NW values, these windows concentrate in a similar constant region in time-frequency plane as that of Hermite functions.

In the way the MW-TFA is implemented, it is the natural extension of Thomson's MWM. The MW-TFA performs multiple window spectral estimation in a piecewise fashion. Within a given window centered in time t, it uses the Thomson's MWM to estimate the spectrum at time t. Hence, it is still a problem of spectral estimation of the time-limited signal. Since the Slepian sequences are optimal for the analysis of time-limited signals, for matching windows in time domain for Slepian sequences and Hermite functions, the estimation using Slepian sequences should give better estimates. The Hermite functions and associated eigenvalues, however, are much easier to calculate in practice. We used fixed sliding windows for the MW-TFA and the windows were needed to be calculated only once. As mentioned in Section 5.2.3, adaptive windows may be necessary to capture time varying components in the signal. In this case, the simplicity of calculation of the Hermite functions might outweigh the loss of optimality.

The MW-TFA is a technique that is still in a state of development. Recently, Friedlander and Scharf (personal communication) have developed a more general form of MW-TFA. However, the design of the windows has not been addressed yet.

Chapter 6

Conclusions

Time-frequency analysis of EEG has been used to monitor neuronal oscillations in two strongly connected brain structures: the entorhinal cortex and the hippocampus. We have also used time-frequency coherence functions (Equations 4.4 and 5.8) to investigate the temporal relationships between rhythmic activities in the two sites. By applying various frequencies of stimulation to the piriform cortex, we found:

- The response of these structures to stimulation trains occurred most strongly near 15 Hz. This suggests that rhythmic activity near 15 Hz may play an important role in gating the olfactory input to the hippocampus via the entorhinal cortex.

- The coherence between the EEG signals recorded from these sites was found to increase monotonically with stimulation frequency up to about 35 Hz. This indicates although the neural signals above 15 Hz were reduced in magnitude, their phase coupling was even more consistent.

The time-frequency analysis used in the thesis provided an effective tool for investigating the role that oscillatory states play in determining the flow of neuronal activity between brain sites.

We used several time-frequency analysis methods to study the EEG signals. These methods include the STFT, WVD and MW-TFA. The WVD offered the highest resolution in both time and frequency among these methods, but its cross-terms and negative values made it difficult to interpret the results. The MW-TFA produced a low bias and low variance estimation of the time-frequency distribution, given only *one realization* of data, but it had poorer time and frequency resolution than the STFT. The STFT provided a time-frequency presentation with no cross-terms and reasonably good time and frequency resolution; it seems to be the most suitable method for the stimulation-induced signals studied in this thesis. For the spontaneous EEG, which is both stochastic and nonstationary, the MW-TFA would be a better choice than the STFT.

We also compared the performance of the MW-TFA using Slepian sequences and Hermite functions. By carefully matching the two window functions, we found there was no noticeable difference in time-frequency plane between them. Although the Slepian sequences are the optimal windows, the Hermite functions would be more suitable when adaptive windows are needed owing to their simplicity in calculation.

Publications related to this thesis work

Haykin, S., Racine, R. J., Xu, Y. and Chapman, C. A. (1996). Monitoring neuronal oscillations and signal transmission between cortical regions using time-frequency analysis of electroencephalographic activity. *Proceedings of the IEEE*, 84(9):1295-1301.

Xu, Y., Haykin, S., Racine, R. J. and Chapman, C. A. (1994). Time-frequency analysis of EEG from entorhinal cortex and dentate gyrus. *Society for Neuroscience Abstract*,20:1434.

Chapman, C. A., Xu, Y., Haykin, S. and Racine, R. J. (submitted). Beta-frequency (15-35 Hz) EEG activities elicited by toluene and electrical stimulation in the behaving rat. *Neuroscience*

Xu, Y., Haykin, S. and Racine, R. J. (in preparation). Multiple window time-frequency analysis of EEG using Slepian sequences and Hermite functions. *Signal Processing Letters.*

Bibliography

Adey, W. R., Kado, R. T., and Walter, D. O. (1967). Computer analysis of EEG data from Gemini flight GT-7. *Aerospace Medicine*, 38:345–359.

Bayram, M. (1996). Multiple window time-frequency analysis. Master's thesis, Department of Electrical and Computer Engineering, Rice University.

Berger, H. (1929). Uber das elektrenkephalogramm des menschen. *Archiv fur Psychiatrie und Nervenkrankheiten*, 87:527–570.

Bland, B. H. (1986). The physiology and pharmacology of hippocampal formation theta rhythms. *Progress in Neurobiology*, 26:1–54.

Boashash, B. (1991). Time-frequency signal analysis. In Haykin, S., editor, *Advances in Spectrum Analysis and Array Processing*, volume 1, chapter 9, pages 418–517. Prentice-Hall: Englewood Cliffs, NJ.

Boeijinga, P. H. and Lopes da Silva, F. H. (1989). Modulations of EEG activity in the entorhinal cortex and forebrain olfactory areas during odour sampling. *Brain Research*, 478:257–268.

Bressler, S. L. (1984). Spatial properties of EEG's from olfactory bulb and cortex. *Electroencephalography and Clinical Neurophysiology*, 57:270–276.

Bressler, S. L. (1990). The gamma wave: a cortical information carrier? *Trends in Neurosciences*, 13:161–162.

Chapman, C. A. and Racine, R. J. (1997). Synaptic plasticity in piriform cortex efferents to the entorhinal cortex in vivo: kindling-induced potentiation and the enhancement of long-term potentiation by low-frequency piriform cortex or medial septal stimulation. *Hippocampus*, 7:257–270.

Chapman, C. A., Xu, Y., Haykin, S., and Racine, R. J. (submitted, 1997). Beta-frequency (15-35 Hz) EEG activities elicited by toluene and electrical stimulation in the behaving rat. *Neuroscience*.

Choi, H.-I. and Williams, W. J. (1989). Improved time-frequency representation of multi-component signals using exponential kernel. *IEEE Transactions on Acoustic Speech and Signal Processing*, 37:862–871.

Cohen, L. (1989). Time-frequency distributions - A review. *Proceedings of the IEEE*, 77:941–981.

Cohen, L. (1995). *Time-frequency Analysis.* Prentice-Hall:London.

Daubechies, I. (1988). Time-frequency localization operators: a geometric phase space approach. *IEEE Transactions on Information Theory*, 34:605–612.

Dumermuth, G. and Molinari, L. (1987). Spectral analysis of EEG background activity. In Gevins, A. and Remond, A., editors, *Handbook of Electroencephalography and Clinical Neurophysiology*, volume 1, pages 85–130. Elsevier: Amsterdam.

Dutertre, F. (1974). Catalogue of the main EEG pattern. In Remond, A., editor, *Handbook of Electroencephalography and Clinical Neurophysiology*, volume 11, part A, pages 40–79. Elsevier: Amsterdam.

Ehlers, C. L., Wall, T. L., and Schuckit, M. A. (1987). EEG spectral characteristics following ethnol administration in young men. *Electroencephalography and Clinical Neurophysiololgy*, 73:179–187.

Fein, G., Raz, J., Brown, F. F., and Merrin, E. L. (1988). Common reference coherence data are confunded by power and phase effect. *Electroencephalography and Clinical Neurophysiology*, 69:581–584.

Frazer, G. and Boashash, B. (1994). Multiple window spectrogram and time-frequency distributions. *Proceedings of IEEE International Conference on Acoustic, Speech, and Signal Processing-ICASSP'94*, IV:293–296.

Freeman, W. J. (1978). Spatial properties of an EEG event in the olfactory bulb and cortex. *Electroencephalography and Clinical Neurophysiology*, 44:586–605.

Freeman, W. J. and Schneider, W. (1982). Changes in spatial patterns of rabbit olfactory EEG with conditioning to odors. *Psychophysiology*, 19:44–56.

Gath, A., Feuerstein, C., Pham, D. T., and Rondouin, G. (1992). On the tracking of rapid dynamic changes in seizure EEG. *IEEE Transactions on Biomedical Engineering*, 39:952–958.

Gersch, W. (1987). Nonstationary multichannel time series analysis. In Gevins, A. and Remond, A., editors, *Handbook of Electroencephalography and Clinical Neurophysiology*, volume 2, pages 261–296. Elsevier: Amsterdam.

Haykin, S. and Bhattacharya, T. (1997). Modular learning strategy for signal detection in nonstationary environment. *IEEE Transactions on Signal Processing*, 45:1619–1636.

Haykin, S., Racine, R. J., Xu, Y., and Chapman, C. A. (1996). Monitoring neuronal oscillations and signal transmission between cortical regions using time-frequency analysis of electroencephalographic activity. *Proceedings of the IEEE*, 84(9):1295–1301.

Heale, V. R., Vanderwolf, C. H., and Kavaliers, M. (1994). Components of weasel and fox ordors elicit fast wave bursts in the dentate gyrus. *Behavioural Brain Research*, 63:159–165.

Hebb, D. O. (1949). *The Organization of Behavior: A Neuropsychological Theory.* Wiley: New York.

Hlawatsch, F. and Boudreaux-Bartels, G. F. (1992). Linear and quadratic time-frequency signal representations. *IEEE Signal Processing Magazine*, 9:21–67.

Hogan, K. and Fitzpatrick, J. (1988). The cerebral origin of the alpha rhythm. *Electroencephalogray and Clinical Neurophysiology*, 69:79–88.

Jeong, J. and Williams, W. J. (1992). Kernel design for reduced interference distribution. *IEEE transactions on Signal processing*, 40:402–412.

Kawabata, N. (1973). A nonstationary analysis of the electroencephalogram. *IEEE Transactions on Biomedical Endineering*, 20:444–452.

Knott, J. R., Gibbs, F. A., and Henry, C. E. (1842). Fourier transforms of electroencephalogram during sleep. *Journal of Experimental Psychology*, 31:465–477.

Lopes da Silva, F. (1991). Neural mechanisms underlying brain waves: from neural memberanes to networks. *Electroencephalography and Clinical Neurophysiology*, 79:81–93.

Lopes da Silva, F., Witter, M. P., Boeijinga, P. H., and Lohman, A. H. M. (1990). Anatomical organization and physiology of the limbic cortex. *Physiological Reviews*, 70:81–93.

Marple, S. L. (1987). *Digital Spectral Analysis with Applications.* Prentice-Hall: Englewood Cliffs, NJ.

Martin, W. and Flandrin, P. (1985). Wigner-Ville spectral analysis of nonstationary process. *IEEE Transactions in Acoustic, Speech, and Signal processing*, 33:1461–1470.

Michel, C. M., Lehmann, D., Henggeler, B., and Brandeis, D. (1992). Localization of the sources of EEG delta, theta, alpha and beta frequency bands using the FFT dipole approximation. *Electroencephalography and Clinical Neurophysiology*, 82:38–44.

Scheuler, W., Rappelsberger, P., Schmatz, F., Pastelak-Price, C., Petsche, H., and Kubicki, S. (1990). Periodicity analysis of sleep EEG in the second and minute ranges - example of application in different alpha activities in sleep. *Electroencephalography and Clinical Neurophysiology*, 76:222–234.

Shaw, J. C. (1984). Correlation and coherence analysis of the EEG: a selective tutorial review. *International Journal of Psychophysiology*, 1:255–266.

Singer, W. (1993). Synchronization of cortical activity and its putative role in information processing and learning. *Annual Review of Physiology*, 55:349–374.

Slepian, D. (1978). Prolate spheroidal wave functions, Fourier analysis, and uncertanty-V: The discrete case. *The Bell System Technical Journal*, 57:1371–1430.

Steriade, M., Gloor, P., Llinas, R. R., Lopes da Silva, F. H., and Mesulam, M.-M. (1990). Basis mechanisms of cerebral rhythmic activities. *Electroencephalography and Clinical Neurophysiology*, 76:481–508.

Sugimoto, H., Ishii, N., Iwata, A., Suzumura, N., and Tomita, T. (1978). On the stationarity and normality of the electroencephalographic data during sleep stages. *Computer Programs in Biomedicine*, 8:224–234.

Thomson, D. J. (1982). Spectrum estimation and harmonic analysis. *Proceedings of the IEEE*, 70:1055–1096.

Vanderwolf, C. H. (1969). The hippocampal electrical activity and voluntary movement in the rat. *Electroencephalography and Clinical Neurophysiology*, 26:407–418.

Vanderwolf, C. H. (1992). Hippocampal activity, olfaction, and sniff: an olfactory input to the dentate gyrus. *Brain Research*, 593:197–208.

Witter, M. P., Groenewegen, H. J., and Lopes da Silva, F. H. (1889). Functional organization of the extrinsic and intrinsic circuitry of the parahippocampal region. *Progress in Neurobiology*, 33:161–253.

Xu, Y., Haykin, S., Racine, R. J., and Chapman, C. A. (1994). Time-frequency analysis of EEG from entorhinal cortex and dentate gyrus. *Society for Neuroscience Abstract*, 20:1434.

Zaveri, H. P., Williams, W. J., Iasemidis, L. D., and Sackellares, J. C. (1992). Time-frequency representation of electrocorticaograms in temporal lobe epilepsy. *IEEE Transactions on Biomedical Engineering*, 39:502–509.